TOPICAL REVIEW • OPEN ACCESS

Dynamically customizable 4D printed shape memory polymer biomedical devices: a review

View the article online for updates and enhancements.

MATERIALS FUTURES

Topical Review

Dynamically customizable 4D printed shape memory polymer biomedical devices: a review

Xiaozhou Xin[1,4]**, Cheng Lin**[2,4]**, Xiaofei Wang**[2]**, Fukai Liu**[3]**, Lili Dong**[3]**, Liwu Liu**[1,*]**, Yanju Liu**[1,*] **and Jinsong Leng**[2]

[1] Department of Astronautical Science and Mechanics, Harbin Institute of Technology, Harbin, People's Republic of China
[2] Centre for Composite Materials and Structures, Harbin Institute of Technology, Harbin, People's Republic of China
[3] Animal Laboratory Center, The First Affiliated Hospital of Harbin Medical University, Harbin, People's Republic of China

E-mail: yj_liu@hit.edu.cn and liuliwu_006@163.com

CrossMark

Abstract
There is an increased risk of complications and even surgical failures for various types of medical devices due to difficult to control configurations and performances, incomplete deployments, etc. Shape memory polymers (SMPs)-based 4D printing technology offers the opportunity to create dynamic, personalized, and accurately controllable biomedical devices with complex configurations. SMPs, typical representatives of intelligent materials, are capable of programmable deformation in response to stimuli and dynamic remodeling on demand. 4D printed SMP medical devices not only enable active control of configuration, performance and functionality, but also open the way for minimally invasive treatments and remote controllable deployment. Here, the shape memory mechanism, actuation methods, and printing strategies of active programmable SMPs are reviewed, and cutting-edge advances of 4D printed SMPs in the fields such as bone scaffolds, tracheal stents, cardiovascular stents, cell morphological regulation, and drug delivery are highlighted. In addition, promising and meaningful future research directions for 4D printed SMP biomedical devices are discussed. The development of 4D printed SMP medical devices is inseparable from the in-depth cooperation between doctors

---

[4] These authors contributed equally to this work.
[*] Authors to whom any correspondence should be addressed.

1

and engineers. The application of 4D printed SMP medical devices will facilitate the rapid realization of 'smart medical care' and accelerate the process of 'intelligentization' of medical devices.

1. Introduction

Shape memory polymers (SMPs) are a class of stimuli-responsive intelligent materials that are able to program to a temporary configuration and recover to the initial configuration when exposed to external stimuli (e.g. heat, light, water/humidity, magnetic fields, and electricity) [1–12]. The shape transformation capabilities of SMPs give them advancements in structure and performance, which have shown promising application potential in aerospace, textile manufacturing, flexible electronics, soft robotics, and other fields [13–16]. Bio-based SMPs, such as shape memory polylactic acid (PLA), shape memory polyurethane (PU), and shape memory polycaprolactone (PCL), have attracted much attention in the biomedical field due to their excellent biodegradability, biocompatibility, deployment adaptivity, and remote controllability [10, 17, 18]. They have shown broad application prospects in implantable tissue engineering scaffolds [19, 20], occlusion devices [21], self-tightening sutures [22], drug delivery devices [23], orthopedic fixation devices, etc [24, 25]. Hu *et al* developed a shape memory PU (SMPU)/hydroxyapatite (HA) foam for bone repair. The compressed SMP foam reduced implantation trauma, enabled adaptive deployment in animals, and automatically matched the edges of bone defects. Histological analysis showed that the foam contributed to vascularization and bone reconstruction [26].

3D printing is a technique to create 3D constructs by adding materials layer by layer through computer-aided design [27–35]. 3D printing has brought the manufacturing industry the ability to accurately prepare complex structures and the flexibility of digitalization, and its applications have spread throughout aerospace, biomedical, archeology, education, architecture, etc [28, 29, 36–42]. In particular, 3D printing has gained rapid development in tissue engineering and regenerative medicine due to its capability to customize human tissues, organs, and tissue engineering scaffolds with complicated structures [43–46]. Combined with imaging technology, it can reproduce personalized implants of host anatomical structures, enabling precision medicine [47–53].

However, 3D printed structures are static, and their structures or properties cannot be automatically reshaped after forming, which seriously hinders their functions and applications. 4D printing technology adds the dimension of transformation over time, allowing 3D printed structures to actively and dynamically change in shape or properties [54–63]. 4D printing can be achieved by using intelligent materials (e.g. SMPs) as raw materials for 3D printing [64–71]. The emergence of 4D printing provides an effective solution to the problem that 3D printing structures are difficult to reshape performance and functionality [20, 72–76]. The advantages of 4D printing SMP in the biomedical field include personalized customization of configuration and performance, adaptive and remotely controllable deployment, minimally invasive implantation, multifunctionality, etc [77–79], which are explained in detail as follows: (a) the use of 4D printing to prepare tissue-engineered scaffolds enables the scaffolds to have a patient-tailored configuration, effectively avoiding complications such as wear and tear of the surrounding tissues, displacement, and embolism due to the unsuitable size of the scaffolds. In addition, combined with structural design such as metamaterials, through the adjustment of structural parameters, the mechanical properties of medical devices can be customized to match human tissues; (b) the tissue scaffold can automatically match the defect contour during the deformation process, and is particularly suitable for the repair of special-shaped defects, such as irregular-shaped bone defects. Besides, the active deformation characteristics of 4D printed SMPs enable remote deployment and the ability to automatically deploy in a controlled manner in hard-to-reach locations *in vivo*; (c) the programmable characteristics and temporary configuration flexibility of 4D printed SMP enable minimally invasive implantation. For example, the temporary configuration of tissue scaffolds can be programmed into low-profile/small cross-sectional area structures to facilitate minimally invasive implantation; (d) 4D printed SMPs are able to embed additional functionality in medical devices. For example, 4D printed SMP drug-loaded medical devices are programmed and the deformation process is associated with the drug release behavior of the device. Therefore, the drug behavior can be controlled and adjusted through changes in structure/performance during SMP deformation. In addition, combining with the concept of wearable electronics and endowing 4D printed medical devices with monitoring functions is poised to become a significant trend in the future development of smart medical devices [80]. In summary, the application of 4D printed SMP medical devices is expected to help promote significant innovation and intelligent development in the field of medical devices, which can significantly reduce the complication rate and improve the success rate of surgery.

Here, we provide a comprehensive summary and in-depth analysis of the strengths and limitations ranging from SMP actuation strategies and printing methods to 4D printed SMP
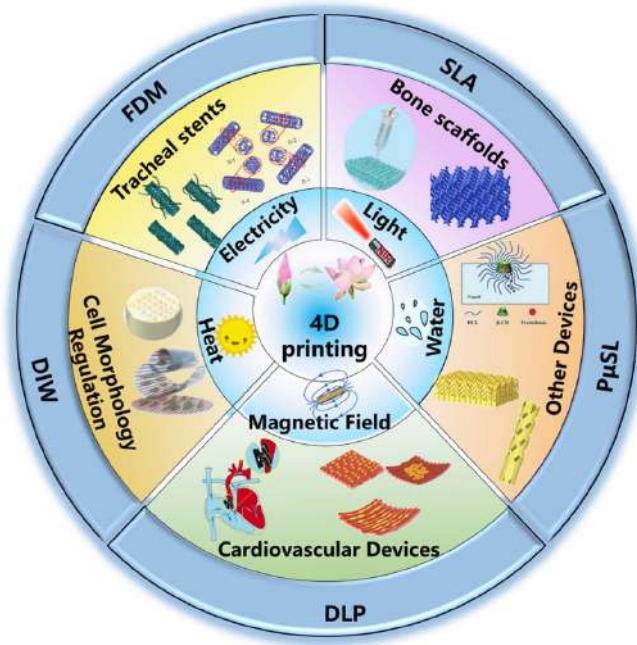
Figure 1. Graphical overview of biomedical applications of 4D printed SMPs. The actuation methods for 4D printed SMP biomedical devices mainly include heat, light, water/humidity, and magnetic field. 4D printed SMPs have demonstrated their promising application potential in bone scaffolds, tracheal stents, cardiovascular devices, cell morphological regulation, etc. The implementation strategies of 4D printed SMPs include fused deposition modeling (FDM), direct writing (DIW), stereo lithography appearance (SLA), digital light processing (DLP) and projection micro stereolithography (PµSL). [2] John Wiley & Sons. © 2022 Wiley-VCH GmbH. [72] John Wiley & Sons. © 2020 Wiley-VCH Verlag GmbH & Co. KGaA, Weinheim. Reprinted with permission from [74]. Copyright (2020) American Chemical Society. Reprinted with permission from [81]. Copyright (2021) American Chemical Society. Reproduced from [82]. © IOP Publishing Ltd All rights reserved. Reprinted from [83], © 2022 Elsevier Ltd All rights reserved. Reprinted from [84], © 2019 Elsevier Ltd All rights reserved. Reprinted with permission from [85]. Copyright (2021) American Chemical Society. Reprinted from [86], © 2024 Elsevier B.V. All rights reserved. Reprinted from [87], © 2020 Elsevier B.V. All rights reserved.

medical devices, which is rare in the previous reviews. Specifically, we elucidate technical considerations related to printing strategies, SMP biomaterials, and stimuli used to actively trigger configuration changes in biomedical devices. The current state-of-the-art 4D printed SMPs for biomedical devices, including bone scaffolds, tracheal stents, cardiovascular devices, cell morphological regulation, etc, were introduced in detail. The challenges of 4D printed SMP materials for biomedical applications are pointed out, and the advantages and limitations of various 4D printed SMP preparation strategies are described. Finally, the challenges of 4D printed SMP in biomedical field are analyzed and summarized, and the future research focuses and promising development directions are deeply analyzed. Figure 1 shows a graphical overview of biomedical applications of 4D printed SMPs.

2. SMPs

2.1. Shape memory mechanism

The shape memory effect (SME) of the SMP results from the combination of the fixed phase and the switchable phase. The switchable phase is movable molecular chains that can be reversibly activated or frozen, which determines the shape fixation property of SMP. The critical temperature at which the switchable phase switches between the 'active state' or 'frozen state' is the shape memory transition temperature (T_{trans}) of SMP. T_{trans} is determined by the glass transition temperature (T_g) or melting temperature (T_m). The fixed phase can be the physical cross-linking points formed by the entanglement of polymer chains or the chemical cross-linking points formed by covalent bonds, which can 'remember' the initial configuration of SMP and ensure the shape recovery process.

The typical shape memory mechanism (taking the thermally actuated SMP as an example) is as follows (figure 2). At room temperature, the molecular chains in SMP are freely arranged with the highest entropy. When SMP is heated above T_{trans}, the switchable phase will be activated, and the molecular chain mobility will increase. Thus, SMP can be easily programmed into the required temporary configuration by applying loads. After cooling below T_{trans}, the molecular chains of the switchable phase will be oriented and frozen along the loading direction. The temporary configuration of the SMP will be fixed and the oriented molecular chains lead to a decrease in the entropy of the SMP system. When SMP is reheated, the molecular chains will be activated again. Since all thermodynamic systems have a tendency to automatically transform to the entropy-increasing state, the molecular chains will automatically recover to the original non-oriented state due to the presence of the fixed phase, which is macroscopically expressed as a return to the initial configuration of SMP [88].

2.2. Two-way (2W) and multiple SMPs

Based on whether the shape memory process is reversible, SMPs are divided into one-way (1W) and 2W SMPs. The SMPs commonly referred to are 1W-SMPs, in which the shape memory transformation process during a shape memory cycle is unidirectional and irreversible. Under external stimuli, the structure transforms from its initial configuration to a temporary configuration, and then returns to its initial configuration upon receiving the stimulus again, completing a shape memory cycle. The irreversible characteristic refers to the inability of the structure to autonomously revert from its initial configuration to the temporary configuration, necessitating manual intervention for this transition. When SMPs possess more than one stable temporary configuration, they are referred to as multiple SMPs. During a shape memory cycle, triple SMP can remember two temporary configurations, quadruple SMP can remember three temporary configurations, and so forth. The realization of multiple SMEs can be achieved through the synthesis of materials that exhibit a broad transition temperature range or possess two or more distinct phase
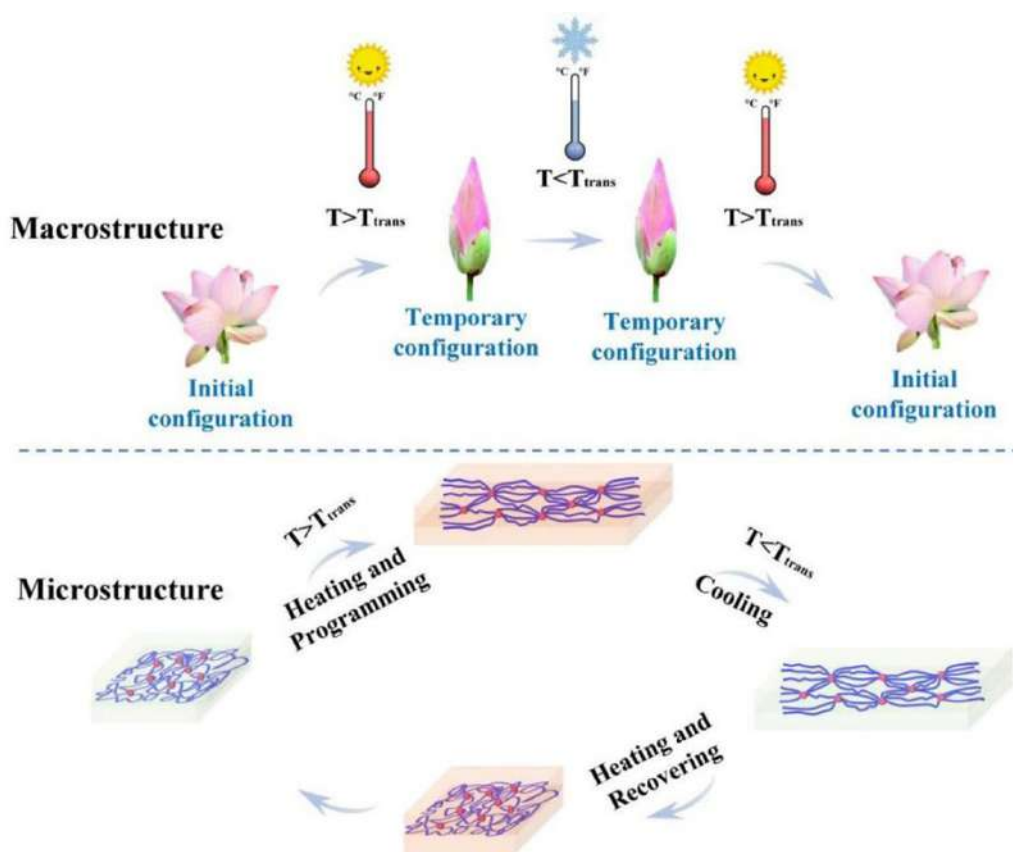
Figure 2. Shape memory mechanism of thermal-actuated SMP (●crosslinking points, ▱ frozen molecular chains, ▱ activated molecular chains).

transitions. For example, the crosslinking of Hexamethylene diisocyanate with poly(ethylene-co-vinyl alcohol) (EVOH), along with the incorporation of FeTA nanoparticles, facilitated the development of a light-driven triple SMP composite (figure 3(a)). The EVOH with two independent phase transition temperatures and the cross-linked network ensured excellent tri-SME. The cross-linked network demonstrated exceptional light-driven recovery stress, capable of withstanding a load 1600 times its own weight. Additionally, combining various stimulus-responsive SMPs to form physical composite structures is an effective approach to achieving multiple SMEs [89].

In contrast to 1W-SMPs, 2W-SMPs exhibited a reversible SME, enabling seamless transitions between temporary and original configurations without the necessity for manual reprogramming, greatly enhancing their applicability across various domains. Typically, 2W-SME is achieved by synthesizing physically or chemically cross-linked semi-crystalline polymer networks, or by physically compositing dual-layer materials. A cross-linked semi-crystalline network exhibiting both 1W- and 2W-SME was designed and synthesized using methacrylate-terminated polyethylene glycol (PEG) in conjunction with butyl acrylate (BA). By exploiting the extensive molecular weight distribution of PEG (2–10 kDa), precise modulation of the transition temperature in proximity to physiological conditions can be achieved, alongside a broad

spectrum of transition temperatures. The results showed that the cross-linked PEG-2,4,10k network exhibited 2W-SME at physiological temperature and 0 °C, with 2W shape memory recovery rates of 8.2% and 6.2%, respectively. Interestingly, while maintaining 2W-SME, the cross-linked PEG-2,4,10k network also exhibited water/humidity responsive properties, with a recovery rate of up to 98%. The cross-linked PEG-2,4,10k network demonstrated preliminary potential for applications in the biomedical field, including minimally invasive implantable devices and sutures (figure 3(b)).

Besides, water-driven 2W-SMP crosslinked network was synthesized by free radical polymerization using vinyl-ended 6-arm poly(ethylene glycol)-poly(ε-caprolactone) (6-arm PEGCL-AC) and vinyl-ended Pluronic F127 (PF127-AC). PCL and PF127 possessed distinct crystalline domains, and the differential hydrophobicity along with their asymmetric chemical structures conferred the cross-linked network with a 2W-SME. In aqueous environments, the crystalline domain of PF127 underwent complete disintegration at room temperature, whereas the crystalline domain of PCL remained intact. The reversible crosslinked network exhibited a maximum reversibility of 45.2%, indicating significant potential for applications in robotics and biomedical fields [91].

In fact, the 2W-SMP that is suitable for biological applications, especially in-body implantable devices, is challenging because the temperature transition range needs to be strictly
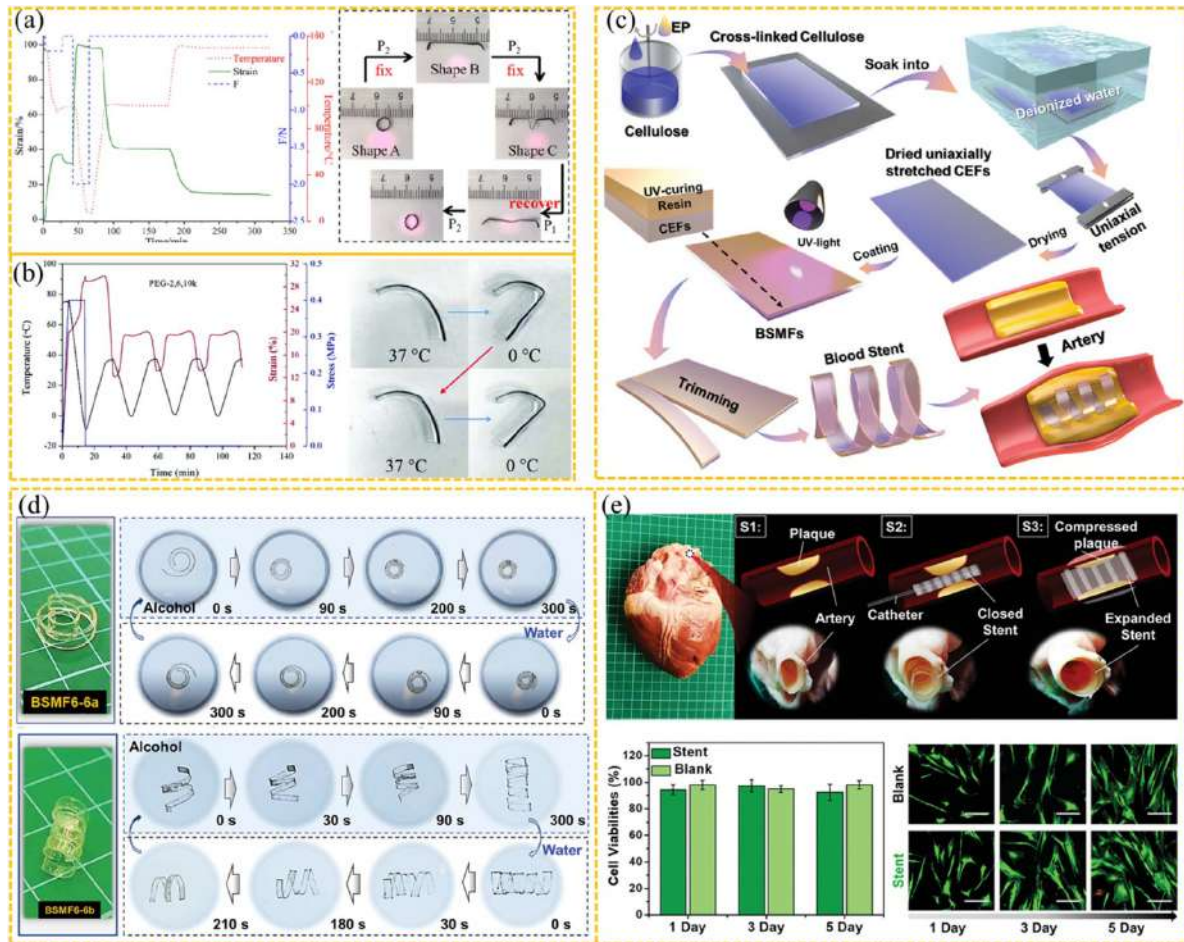
Figure 3. (a) Shape memory cycling curves and light-actuated triple shape memory behavior of EVOH-FeTA triple SMP composite [89]. Reproduced from [89], with permission from American Chemical Society. (b) Reversible shape-memory effect of cross-linked PEG-2,4,10k network and its reversible transformation behavior at body temperature and 0 °C. Reprinted with permission from [89]. Copyright (2021) American Chemical Society. (c)–(e) Two-Way shape memory BSMFs. (c) Schematic diagram of preparation and application of BSMF. (d) Shape change process of BSMFs with different structure. (e) BSMFs exhibited excellent biocompatibility [90]. [90] John Wiley & Sons. © 2021 Wiley-VCH GmbH.

controlled. Based on the tunability of crystallization thermodynamics in the driving domain, POA-dimethacrylate (DA) and PCL-DA were copolymerized to form a semi-crystalline crosslinked network with reversible SME within a narrow temperature range. Reversible actuation can be achieved within a temperature range of 24 °C, with boundary temperatures of 43 °C and 19 °C, both of which fall within the physiological temperature range suitable for human applications. The cross-linked network demonstrated a reversible strain of 17%, highlighting its potential as a non-permanent implant actuator for micro medical robots designed for drug release and retrieval applications [92].

For bidirectional SMPs applied in the field of biology, gentle driving methods and excellent biocompatibility are crucial. Biocompatible cellulose was employed as the raw material to synthesize BSMF with varying structural configurations. It demonstrated exceptional curling and swelling characteristics under mild stimulation and exhibited superior cellular compatibility, indicating significant application potential in the domain of vascular stents (figures 3(c)–(e)) [90].

2.3. Actuation methods

2.3.1. Thermally actuated SMPs.
Thermally actuated SMPs have been extensively studied [49, 93, 94]. However, direct heating to actuate SMPs is sometimes difficult to control or difficult to implement [88]. Indirect actuation methods, including magnetic-, light-, water/humidity-, and electrical-actuation, give flexibility and controllability to the deformation of SMPs and further broaden the scope of SMP applications [95–102].

2.3.2. Magnetically actuated SMPs.
Magnetically actuated shape recovery of SMPs can be achieved by introducing magnetic nanoparticles, such as ferric tetroxide (Fe_3O_4) and iron oxide (Fe_2O_3), into the SMP matrix. The fundamental mechanism involves the generation of hysteresis loss by the magnetic filler in an alternating magnetic field, which is subsequently converted into thermal energy to elevate the temperature of the SMP substrate. Once the temperature of the SMP exceeds its T_{trans}, the SMP will undergo

a shape transformation. A novel magnetically driven shape memory composite material has been developed by integrating micron-sized Fe_3O_4 and NdFeB particles, which exhibits characteristics such as remote rapid actuation, and reconfigurable deformation capabilities. Under high-frequency magnetic fields, Fe_3O_4 particles underwent induction heating, facilitating shape locking and unlocking, whereas NdFeB particles enabled the composite to undergo reconfigurable deformation under the influence of external low-frequency or direct current magnetic fields (figure 4(a)) [8]. Magnetically actuated SMPs are characterized by remote control and selective heating, which are advantageous for non-contact actuation in confined and restricted spaces [103, 104]. Fe_3O_4 nanoparticles have attracted wide attention due to their good biocompatibility and can be cleared by human metabolism [105–108]. Wang *et al* introduced different contents of Fe_3O_4 nanoparticles into the SMP matrix and prepared structures capable of achieving shape recovery in an alternating magnetic field. The shape recovery rate was above 99% at a frequency of 60 kHz and a magnetic field strength of 21.21 kA m^{-1}, and the recovery rate increased rapidly with the increase of nanoparticle content. This magnetically controlled SMP composite was expected to contribute to intravascular transport in MEMS devices [109]. In addition, Fe_3O_4 nanoparticles were introduced into oligomeric (ε-caprolactone) dimethacrylate/BA SMP, which can achieve remote actuation of the shape recovery of the complex structures under alternating magnetic field. The applied magnetic field was within the acceptable treatment window in biomedical applications in terms of frequency and energy, showing its potential in medical and sensing applications [100].

2.3.3. Light-actuated SMPs. The actuation characteristics of light-actuated SMPs are selective, remote, and spatially controllable [88, 98]. According to the different photo-responsive mechanisms, light-actuated SMPs can be divided into photo-chemical responsive SMPs and photothermal responsive SMPs (figures 4(b) and (c)). For photochemical responsive SMPs, the photo-responsive SME is mainly obtained by grafting photo-sensitive molecular groups onto the SMP network, such as azobenzene, spiropyran, cinnamic acid, and coumarin, etc. These photo-sensitive molecular moieties can undergo physical or chemical transformations upon absorbing photons of specific wavelengths, resulting in alterations to the polymer's structure or properties, which subsequently activate the SME of the SMP [111]. For example, cinnamic acid molecules act as molecular switches, and reversible covalent cross-linking of molecular switches is carried out under light to achieve the SME [88, 96]. Azo dyes and spiropyrans undergo reversible structural transformations under different wavelengths of ultraviolet light, thereby inducing SMEs [112, 113].

In addition, the introduction of photothermal fillers into the SMP matrix can also realize the light-actuated shape memory process of SMPs. The photothermal fillers absorb light energy and convert it into thermal energy (i.e. photothermal effect) to trigger the shape memory process. Photothermal fillers include gold nanoparticles (AuNPs) [114], black scale (BP)

[115, 116], graphene oxide (GO) [117, 118], and other synthetic photosensitive particles [99]. PU/BP photothermal composites were prepared by introducing the photothermal filler BP into the piperazine-based SMPU matrix. Under 808 nm near-infrared light (NIR) irradiation, 0.08 wt% BP/PU could rapidly absorb light energy and convert it into thermal energy, triggering the shape recovery process. The columnar PU/BP was implanted into the mouse oviduct and actuated by NIR irradiation. Within 60 s, the PU/BP could gradually return to the initial configuration of short and thick columns from the temporary configuration of thin and long columns. It showed that the shape recovery of PU/BP can be achieved *in vivo* by remote light actuation and demonstrated the feasibility of contraception by blocking the oviduct with columnar PU/BP [98].

2.3.4. Water/humidity-actuated SMPs. There are three main mechanisms involved in the shape memory process induced by water or humidity. (a) The entry of water molecules into the polymer network induces shape recovery, which is caused by the plasticizing effect or the dissolution of the crystalline phase. (b) Swelling caused by the absorption of water molecules by the polymer. The shape change caused by swelling is pronounced in hydrogels. (c) SME associated with the formation of hydrogen bonds between polymer macromolecules and water molecules. The increase in the strength of hydrogen bonds between the polymer and water inhibits the interactions between polymer macromolecules, leading to a decrease in the T_g of the polymer. It also accelerates the release of stored energy inside the polymer, which contributes to shape recovery [97, 102]. The natural water/solution environment in living organisms contributes to the biological application of water/humidity-actuated SMPs. Inspired by the concepts of thermal-induced lattice distortion and phase separation, researchers designed a novel water-triggered hardening SMPU, where the polymer main chain was composed of rigid segments and the side chains were composed of pendant PEG soft segments. Fragment rearrangement facilitates the shape-memory process in the hydrated state of polymers, with enhanced shape recovery ratio. The application of water-triggered shape-memory PU in tissue engineering scaffolds enables effective lumen expansion while maintaining a balance among mechanical properties, shape-memory characteristics, and biocompatibility (figures 5(a) and (b)) [119]. Furthermore, by combining microcrystalline cellulose (MCC) with biodegradable PDLLA, a water-responsive shape-memory composite material (PDLLA/MCC) was successfully developed. The experimental results indicated that the composite material exhibits an excellent SME at 37 °C in water, primarily due to the increased flexibility of the polymer chains from swelling and a reduction in the transformation temperature to body temperature. Cell experiments verified its favorable bioabsorbability and biocompatibility, indicating promising potential for applications in the medical field (figure 5(c)) [120].

A water-actuated shape memory intravascular temporary embolization device was reported. PLA containing radiopaque filler was employed as the inner core, and cross-linked PEG
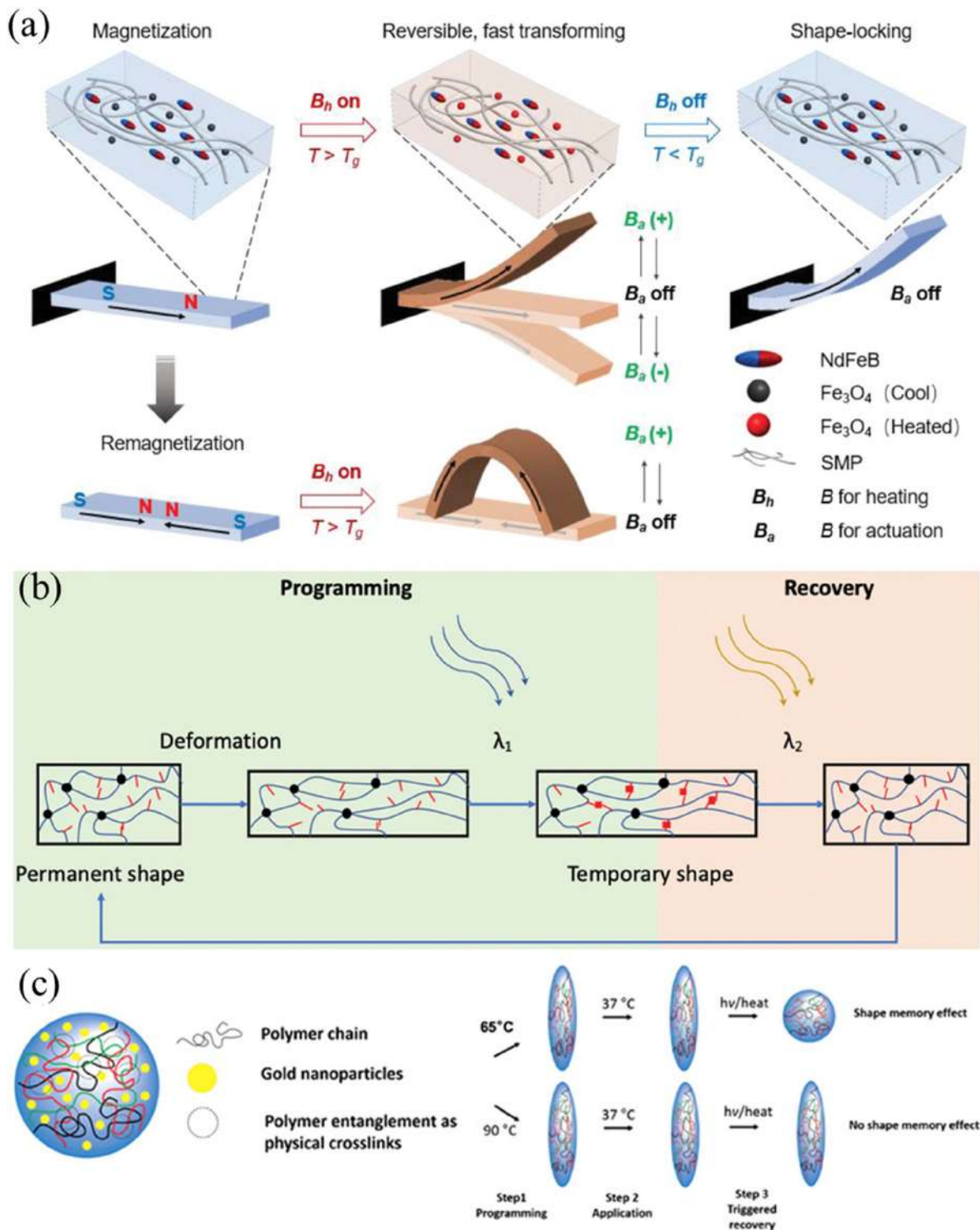
Figure 4. (a) Magnetic responsive shape memory mechanism. [8] John Wiley & Sons. © 2019 WILEY-VCH Verlag GmbH & Co. KGaA, Weinheim. (b) Photochemical responsive SMP shape memory recovery process. [10] John Wiley & Sons. © 2020 WILEY-VCH Verlag GmbH & Co. KGaA, Weinheim. (c) Photothermal responsive SMP shape memory recovery process. Reprinted with permission from [110]. Copyright (2018) American Chemical Society.

hydrogel was employed as the outer layer. The device completed the embolism process within 2 min under the stimulation of body fluid, of which the first ∼60 s was the starting response time, and the last ∼60 s was the embolism process under the joint action of the swelling of PEG hydrogel and the

shape recovery of PLA composite [97]. The shape memory mechanism of PEG in this process was as follows. The chemical covalent cross-linking in PEG hydrogels acted as the fixed phase that determined the shape recovery properties. During programming, the amorphous molecular chains were oriented
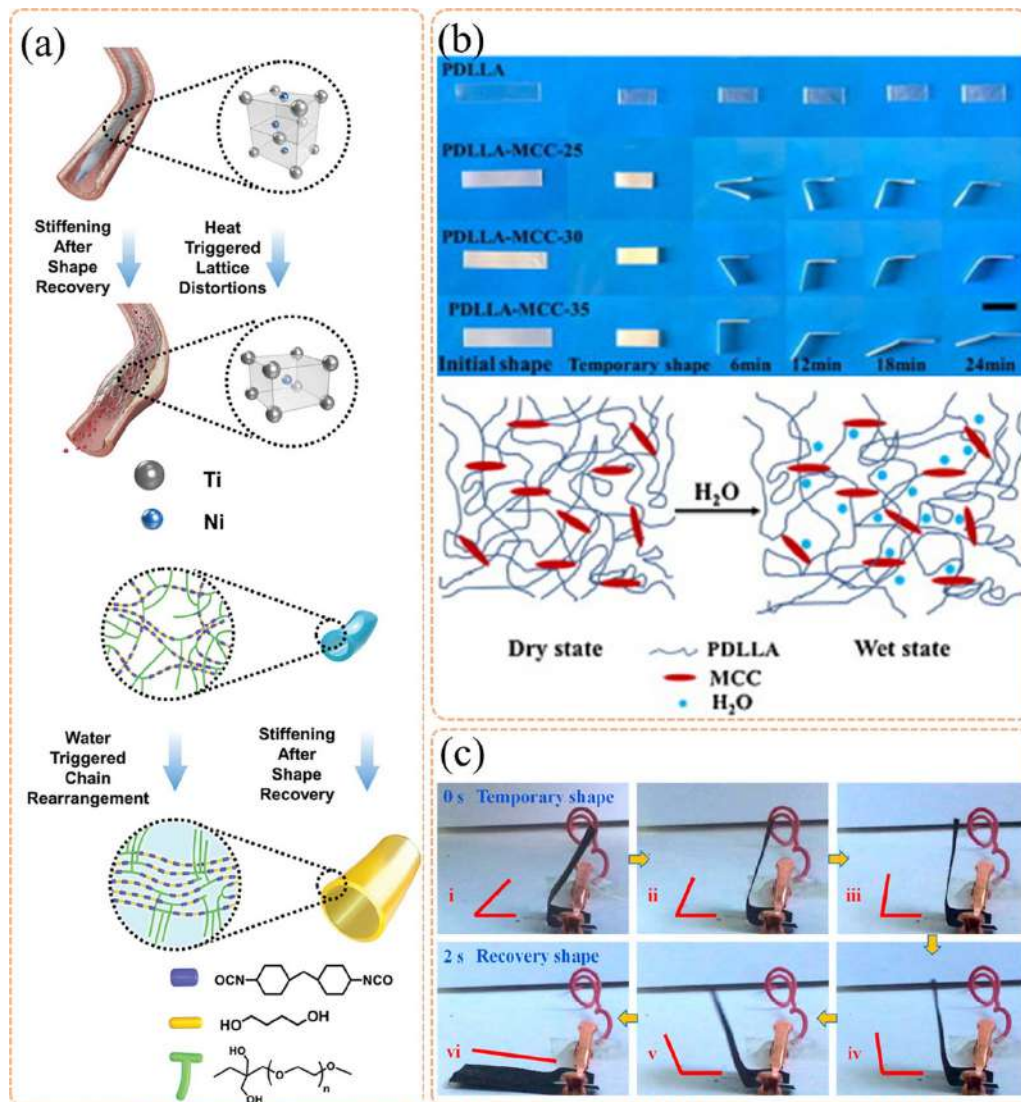
Figure 5. (a) Mechanism of water-induced shape memory process. [119] John Wiley & Sons. © 2022 Wiley-VCH GmbH. (b) Shape memory polyurethane underwent shape recovery to achieve a transformation from soft to hard. Reprinted from [120], Copyright © 2014 Elsevier Ltd All rights reserved. (c) Water-induced shape recovery process and mechanism of PDLLA/MCC. Reprinted with permission from [121]. Copyright (2018) American Chemical Society. (d) Electrically actuated shape memory recovery process.

along the deformation direction and the entropy of the system decreased. After cooling to room temperature, the PEG recrystallized and the crystalline phase acted as a switchable phase, fixing the programmed temporary shape. The PEG was immersed in water at 37 °C and the water molecules diffused into the PEG network and the crystalline phase was dissolved. The network tended to the entropy-increasing state, and gradually returned to the completely amorphous state while swelling, that was, the PEG hydrogel recovered to its initial shape.

2.3.5. Electrically actuated SMPs. Similar to magnetically actuated SMPs, conductive fillers (such as carbon nanotubes, carbon black, and metal nanoparticles) are introduced into the SMP matrix through methods such as doping, embedding,

and coating to prepare electrically actuated SMP composites. Upon the application of an electric voltage, the conductive filler facilitates the conversion of a fraction of electrical energy into thermal energy through the resistive heating effect. This generated heat is subsequently transferred from the conductive filler to the polymer matrix. When the temperature of the SMP exceeds its T_{trans}, it triggers the SME (figure 5(d)) [88, 121]. Electrically actuated SMPs are usually used in soft robots, artificial muscles, etc, but rarely in biomedical fields.

If SMPs are to be used in biomedical devices, actuation temperature and recovery rate are the two most important factors that must be considered for SMPs of all actuation methods. First, in general, the deformation temperature of SMP that can be applied to human body should be between 37 °C–45 °C. If the deformation temperature is too low, the SMP will be in a highly elastic state at body temperature and will

Table 1. Comparison of SMPs actuated by different methods.

Actuation methods	Advantages	Disadvantages
Thermally actuated SMPs [49, 93, 94]	Simple operation, fast response, and diverse shape transformation	It cannot be remotely controlled, and it is difficult to heat in special environments
Magnetically actuated SMPs [103, 104]	Non-contact remote control, selective actuation, fast response	The content of magnetic nanoparticles needs to be controlled to ensure biocompatibility; the types of magnetically responsive materials are limited; alternating magnetic field equipment is bulky and expensive
Light-actuated SMPs [88, 98]	Remote control, non-contact actuation, fast response, selective actuation	The penetration ability of the light source is limited, and the dispersibility of the functional filler is also limite
Water/Humidity-actuated SMPs [97, 102]	Diverse stimulation sources, high safety	Slow response speed and unstable actuation process
Electrically actuated SMPs [88, 121]	Fast response, even heating, and remote operation	Conductive fillers have poor dispersion; limited applications in biological fields

not be able to take advantage of the variable stiffness of the SMP. In particular, it cannot be applied to work conditions that require load-bearing, such as if SMP is used as a vascular stent, it is difficult to open the narrowed blood vessels. If the deformation temperature is too high, it is prone to tissue damage. Despite the rapid recovery of some SMPs ($<$1 min), the effects of localized overheating damage on biological tissues still need to be thoroughly investigated. Non-contact actuation (e.g. magnetic and partially light actuation) is essentially indirect heating, thus strict control of the temperature during deformation is even more important, especially to avoid localized overheating due to uneven dispersion of the functional fillers. Second, adequate recovery of the SMP needs to be ensured. An important feature of SMP tissue scaffolds and other SMP medical devices is that they can actively deform in hard-to-reach areas, so the adequacy of SMP shape recovery is critical. For example, an SMP tracheal stent used to open a collapsed trachea, incomplete recovery of the SMP may result in failure to restore an open airway and surgical failure. The introduction of functional fillers for the preparation of SMP composites is widely used to achieve non-contact actuation, and adequate dispersion of the fillers is important because inhomogeneous dispersion leads to inhomogeneous shape recovery.

In addition, the realization of non-contact actuation, such as magnetic field and light, needs to be considered, and the appropriate actuation strategy needs to be selected in conjunction with the SMP application scenario. Magnetically responsive - SMPs typically require an alternating magnetic field to provide external stimuli and have high requirements for magnetic induction strength and frequency, which greatly limits the size of the magnetic coils. If the magnetically actuated-SMP is to be used for clinical applications, there is a need for the development of large-scale alternating magnetic field equipment, as well as in-depth studies of the effects of alternating magnetic fields on the human body. The additional light source required for light-actuated SMP is more readily achievable, such as near infrared laser, without causing tissue damage.

Thus light-actuated SMP is promising for clinical applications. Water/humidity actuation is also a promising actuation method for practical applications due to the natural liquid environment in the human body. In addition, 4D printing SMP with novel actuation methods is also worth exploring in depth.

A series of near-body temperature SMPs have been developed, but there is still a balance between the transition temperature and the recovery rate. In addition, the possibility of mass production needs to be considered, otherwise highly complex synthetic materials suitable only for the laboratory will still not solve the challenges of practical SMP applications. Furthermore, it is worth noting that although the introduction of functional fillers allows SMPs to respond to external stimuli, the development of intrinsically responsive SMPs is still a direction that needs to be thoroughly investigated. This not only avoids the effect of the introduction of functional fillers on the uniform shape recovery of the SMP, but also improves the printability of the SMP as fillers may clog the nozzle. The comparisons of SMPs actuated by different methods are listed in table 1.

3. Implementation strategy of 4D printing

4D printing can be achieved by 3D printing of SMP materials, and the main printing strategies include fused deposition modeling (FDM), selective laser sintering (SLS), direct writing (DIW), stereo lithography appearance (SLA), digital light processing (DLP), and projection micro stereolithography (PμSL) [59–61].

3.1. FDM

FDM is a filament-based printing strategy. The thermoplastic filament of uniform diameter is sent to the extrusion head for heating through the filament feeding mechanism. The extrusion head moves on the platform and extrudes the material according to the predetermined path. The materials

are deposited layer by layer to complete the construction of the 3D model. The adjustable parameters of the FDM printing strategy include printing speed, layer height, wall thickness, extrusion head temperature, platform temperature, fill density, etc [122–126]. The printing materials used for FDM are thermoplastic polymers. FDM printing materials suitable for biological applications include PLA, PCL, thermoplastic PU (TPU), and various types of nanocomposites based on these materials. For example, ferric oxide-PLA magnetic nanocomposite filaments were prepared, and bone tissues, tracheal scaffolds and cardiac occlusion devices were prepared using FDM printing technology. Meanwhile, it is worth noting that FDM printing of functional filler composites suffers both in terms of printing speed and accuracy due to increased viscosity. In addition, the risk of nozzle clogging increases accordingly.

A wearable personalized oral delivery mouthguard with adjustable release rates was prepared using FDM printing technology. Intraoral scans were performed to obtain the maxillary anatomy for customizing the structure of the mouthguard. A composite printing filament composed of PLA and polyvinyl alcohol (PVA) was fabricated via melt extrusion using a single-screw extruder. Clobetasol propionate (CBS), an anti-inflammatory corticosteroid, was employed as the model drug to address oral inflammation. The suitability of the personalized mouthguard as a drug delivery device was evaluated. Food-grade vanillic acid (VA) was used in place of CBS in human drug release studies. The results showed that the VA was released sustainably during the period of wearing the VA mouthguard. After wearing it for three cycles, the teeth in the area containing VA became significantly white, which verified the effectiveness of the mouthguard as a personalized drug delivery device. By optimizing the printing parameters, the process from scanning in the mouth to wearing the customized mouthguard can be completed within 2 h. Compared with the traditional casting technology, it showed outstanding advantages in manufacturing efficiency and customized structure. In addition, drug-eluting mouthguards that release active compounds over time can reduce salivary flushing or excessive drug use, thereby improving treatment efficacy and reducing side effects [127].

FDM is an effective printing method that has wide applications in various fields. Combining UV technology with 4D printing is an innovation. Under the irradiation of ultraviolet light, the in-situ formation of photo-crosslinking network not only enhances the adhesion strength of each layer but also ensures that the obtained object has good shape memory performance. Various models of modern and classical Chinese architecture, such as figure 6(a), were printed. An adaptive elbow protector and a personalized arm protector were developed using this printing technology, with the Hulk chosen as the model for the protector. Experimental results show that the printed protectors can provide good protection using SME [87].

FDM is the most widely used printing technology because of its simplicity, maneuverability and low cost. Due to the strong openness, modified FDM printers have also become the new favorite of industry and researchers, enabling multimaterial printing. However, FDM printing also faces many challenges. The stepper motor feeding method requires high viscosity and modulus of the printing material, while the pneumatic feeding method is expected to further broaden the selectivity of the printing material. In addition, the printed structure is layered and discontinuous. FDM is prepared in the way of 'from line to surface, from surface to body', there are gaps between the extruded filaments, and there are also gaps between the layers. This results in limited structural continuity and reduced mechanical properties. On the one hand, reducing the nozzle diameter and increasing the feed accuracy can improve the properties of the printed structure. On the other hand, secondary processing can also be used to improve mechanical properties. For example, liquid components can be infiltrated into the interstices of the printed structure to form a 'brick-wall' structure. In terms of printing materials, SMP used for FDM printing is a thermoplastic material, with limited shape recovery rate and shape memory performance after multiple cycles. The incorporation of functional fillers into SMP can enhance additional functionalities, such as drug delivery and radioopacity. However, this addition leads to an increase in the viscosity of the SMP composite, reducing printing speed and accuracy, and increasing the risk of clogging.

3.2. SLS

SLS is an advanced additive manufacturing technology that constructs three-dimensional solid structures by selectively sintering and consolidating powdered materials layer by layer using laser, electron beam, etc [128, 129]. In contrast to FDM, SLS offers significant advantages in the fabrication of intricate hollow structures. During the printing process, the unexposed polymer powder serves as a support medium to ensure the stability of suspended structures, eliminating the need for additional support and base fabrication [94, 129]. SLS is mainly used for the 4D printing of conductive and magnetic SMP composites, therefore, the percentage of nanoparticles is crucial for the printing quality. Due to the limited types of SMPs available for SLS 4D printing technology, the internal structure of the printed object is porous and rough, with a larger surface roughness and limited mechanical properties. To overcome the inherent brittleness of PLA, Pei introduced high elasticity TPU and magnetic nanoparticles Fe_3O_4 into the PLA matrix, and prepared a porous structure TPU/PLA/Fe_3O_4 magnetic-responsive shape memory composite using SLS 4D printing technology. The addition of Fe_3O_4 not only promoted the formation of continuous structure of TPU phase in SMP, improved its mechanical properties, but also endowed the mixture with excellent magnetic shape memory properties, enabling non-contact remote control. Meanwhile, it induced cell proliferation and differentiation, promoted bone regeneration [94, 130].

3.3. DIW

DIW is an additive manufacturing technology that enables the fabrication of 3D structures through predetermined printing paths and pressure-controlled printable inks [131]. The
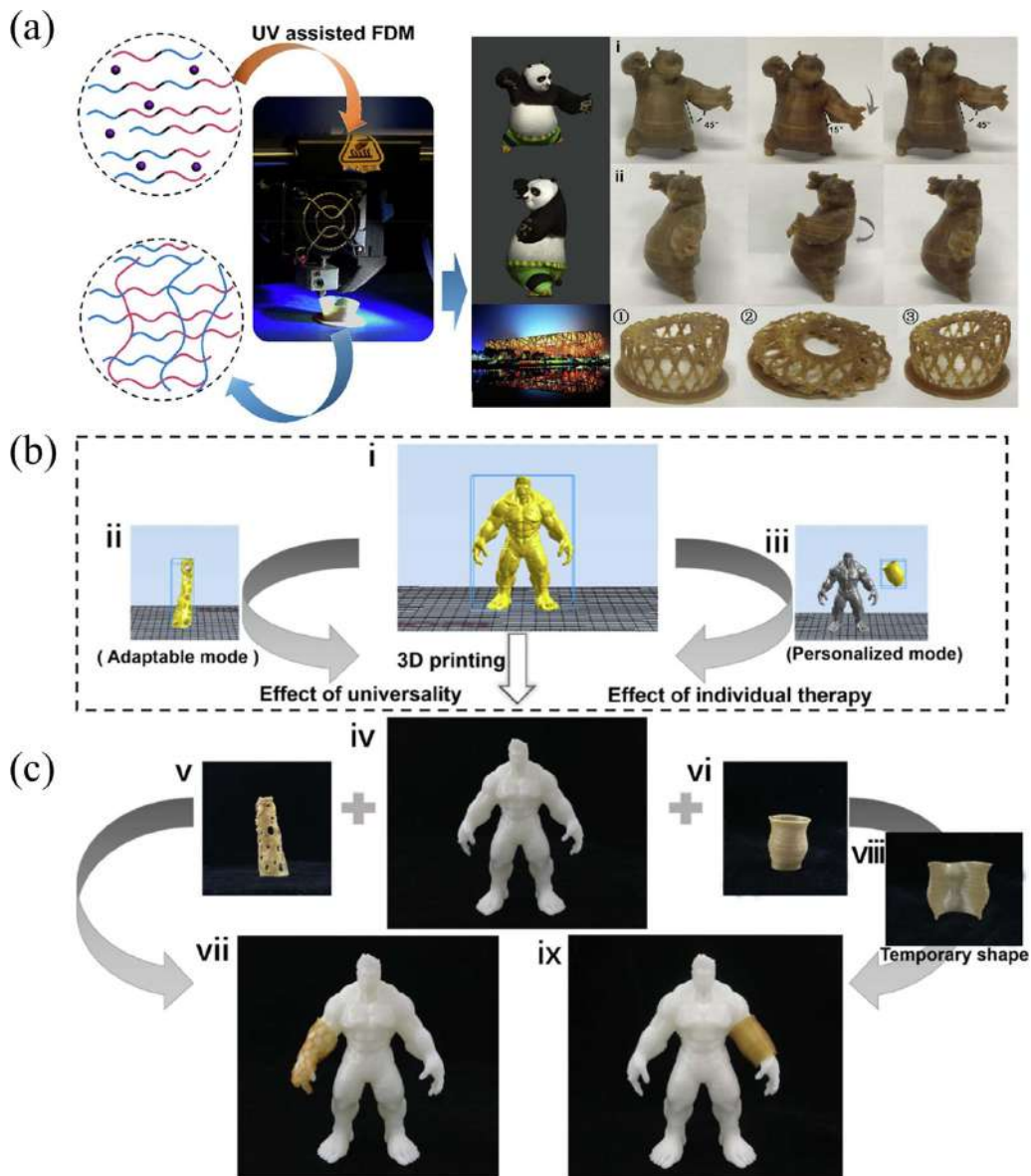
Figure 6. (a) Shape memory process of 4D printing model based on FDM. (b) The slicing software modeling process for the 4D-printed elbow guard. (c) 4D printed elbow support for personalized treatment process. Reprinted from [87], © 2020 Elsevier B.V. All rights reserved.

printing quality of DIW depends on the rheological properties of the printing ink, and the ink with shear thinning behavior and rapid solvent evaporation is an ideal choice. Inks for DIW are widely adjustable and open-ended, enabling control of structure properties by modulating material components [132–149]. The advantages of DIW are good ink openness and the ability to control the structural properties by adjusting the ink composition, but also high requirements for viscosity and conformability. The dissolution of printed materials in volatile solvents and the modulation of the solvent concentration is the most common method of regulating ink viscosity. Adding rheology modifiers and controlling the printing temperature are also effective ways to regulate the viscosity of the ink to improve its printability. In addition, maintaining

the configuration of the printed structure can be achieved by evaporating the solvent and increasing the viscosity of the ink. UV light or post-curing can also be added during the printing process to improve the forming performance. The DIW printing technology requires higher demands on the viscosity and shear thinning behavior of SMP ink, and usually requires post-curing to increase the stability of the structure and enhance the mechanical properties. Wan *et al* prepared poly (D, L-lactide-co-trimethylene carbonate) (PLMC)/poly (trimethylene carbonate) (PTMC) and PLMC/PTMC/Fe_3O_4 inks, and multi-material structures with multi-SME were prepared by DIW. Through selective programming and actuation, the 4D printed multi-material structures exhibited ordered multi-shape transformation with outstanding multi-SME [150].

3.4. SLA

The principle of SLA for manufacturing 3D structures is to scan a liquid bath containing a photosensitive resin (including monomers, prepolymers, and photoinitiators) layer by layer in a point-to-line and line-to-face manner by laser of specific wavelength, which leads to the photopolymerization or cross-linking of the resin [151]. SLA has the advantages of precise control and high resolution, and the light source of SLA can be ultraviolet, infrared, or even visible light. The applicable materials for SLA include PU, acrylate, epoxy resin, etc [152]. The layer height of the laser scanning, the exposure time of each layer, and the resolution of the light source are the main parameters that affect the quality of SLA printing [153, 154]. The biocompatibility of photoinitiators is a critical consideration for enhancing their suitability in biomedical applications. Cells can be encapsulated in the printed scaffold by SLA to obtain scaffolds with high cell density. Since printing materials are not extruded through the injection needles, SLA for biological printing can reduce the risk of cell death due to needle blockage. However, it is still necessary to pay attention to cell damage due to excessive exposure to light. SLA has shown its potential in manufacturing orthodontic devices, hearing aids, functional artificial tissues, drug delivery devices, tissue engineering scaffolds, etc [154, 155]. Abdul *et al* prepared an elastomeric intravesical drug delivery retention device by SLA for the treatment of interstitial cystitis and bladder pain syndrome to achieve targeted bladder therapy and sustained drug release. Two device configurations, solid and hollow, were designed and the devices contained different contents of lidocaine hydrochloride (10%/30%/50%). The results showed that the hollow device could achieve sustained release of lidocaine within 4 d and the solid device could achieve sustained release of lidocaine within 14 d [156].

3.5. DLP

DLP works similarly to SLA, but it is a surface light projection, unlike SLA's point light projection. DLP allows the cross-linking and polymerization of an entire layer of photosensitive material at a time, thus the manufacturing efficiency of DLP is greatly improved, and it has a higher accuracy compared to SLA [157–163]. David *et al* prepared 60 μm high-precision bone tissue engineering scaffolds by continuous DLP technique using polyacrylate fumarate (PPF) as the matrix. The light was attenuated by adding dye titanium dioxide (TiO_2) to the photosensitive resin, and the relationship between TiO_2 concentration and curing thickness was investigated. The TiO_2 competed with the initiator for photons so that the number of photons received by the initiator was reduced, enabling adjustment of the resin curing thickness to increase resolution. High-precision scaffolds may exhibit features that cells can recognize, which was helpful to improve the attachment and proliferation of scaffold-specific cells [164]. However, for DLP, there are also the following disadvantages: Printable materials are limited and costly; there are few types of photoinitiators and their biocompatibility is poor; printed materials are usually cured in a liquid tank, resulting in difficult printing of multiple materials; the openness of the equipment is limited, the release film at the bottom of the printer is easily damaged, and the system maintenance cost is high; after printing, the surface of the structure is not completely cured and requires secondary curing treatment.

Therefore, there is an urgent need to develop photosensitive printable materials with good biocompatibility, strength and toughness. Multi-material printing is expected to be achieved by improving the printer liquid tank, changing the light source irradiation, or designing gradient photosensitive materials through gravity gradients. Design of integrated molding and post-curing equipment with delayed irradiation of the light to achieve automatic post-curing processing.

3.6. PμSL

PμSL is also a surface projection lithography 3D printing technology, but the resolution is much higher than DLP, with resolutions up to several hundred nanometers. However, it is currently only suitable for producing complex 3D structures at the microscale, and its biggest challenge is to improve large image processing and storage techniques to accelerate the practical application of PμSL [165–167]. Furthermore, PμSL necessitates that the printing materials possess low viscosity and superior photo-crosslinking capabilities, resulting in a limited selection of SMPs currently suitable for PμSL. Grigoryan *et al* achieved the printing of monolithic hydrogel structures by PμSL using hydrogels as substrates and food dyes as photoinitiators. Endovascular 3D fluid mixers and functional dolichoid valves were successfully manufactured, which verified the feasibility of food dyes as photoinitiators to prepare hydrogels containing complex and functional vascular topologies [168].

4D printing has shown a broad application prospect in the biomedical field, but different printing methods have their own advantages and limitations (table 2), and there is not a universal printing method. In the future, the combination of several printing methods will be an effective way to improve the application of 4D printing technology, allowing various printing methods to take advantage of their strengths. For various problems in the printing process, current solutions lack theoretical support and are mostly empirical. It is crucial to establish theoretical models between printing parameters and structure performance, which is expected to fundamentally revolutionize the printing technology. In addition, the addition of functional components such as magnetically sensitive/photosensitive particles enables response to external stimuli (magnetic field, light). However, the increase of functional fillers may cause discontinuous printing and nozzle clogging for FDM and DIW. For DLP and SLA, the light transmittance may be affected, causing printing failure. Therefore, it is necessary to develop new intrinsically responsive 4D printing materials.

PLA: polylactic acid; PCL: polycaprolactone; TPU: Thermoplastic polyurethane; PEG: polyethylene glycol; CNT: Carbon nanotubes; GO: Graphite Oxide; Fe_3O_4: ferroferric oxide; PTMC: poly (trimethylene carbonate); PEGDA: poly(ethylene glycol) diacrylate; PCLMA: poly(caprolactone)

Table 2. Comparison of printing strategies.

	Representative biomaterials	Advantages	Disadvantages
FDM [169–172]	PLA, PCL, TPU and their composites, fillers include PEG, CNT, GO, Fe_3O_4, cellulose, etc	The most widely used printing technology, with strong operability, economy, wide sources of materials, good equipment openness, and eco-friendliness	Nozzle clogging, poor bonding, easy to warp, limited printing speed, limited precision, overhanging structure needs to be supported, strictly limited material form (filamentary)
DIW [173, 174]	PLA, PCL, TPU, PTMC, PEGDA, sodium alginate, etc and their composites, fillers including PEG, CNT, GO, Fe_3O_4, cellulose, gelatin, chitosan, HA, etc	High material selectivity, strong material openness	Requiring inks with specific viscosities and shear thinning behavior
SLA [175, 176]	PU, PCL, acrylates, epoxy resins, chitosan, PTMC/Gelatin, PCLMA, etc	High resolution, suitable for complex and hollow structures.	High cost, limited materials, poor biocompatibility of photoinitiators, difficulty in multi-material printing, limited printing efficiency and limited openness of printer
DLP [177–180]	PLA, PCL, PEG, PEGDA, GelMA, SF, polycarbonate acrylate, etc	High precision and efficiency, suitable for printing microstructures	Limited materials, limited biocompatibility of photoinitiators, high cost, difficulty in multi-material printing, limited equipment openness, high maintenance costs, requiring secondary curing treatment
PμSL [181–183]	PPF, PEGDA, etc	Resolution up to several hundred nanometers	Limited materials, high cost, slow printing speed

methacrylate; PPF: polyacrylate fumarate; GelMA: Gelatin Methacryloyl; SF: Silk Fibroin; HA: hydroxyapatite.

4. Applications of 4D printed SMPs in biomedical devices

The emergence of 4D printed SMPs provides an outstanding solution to the problem of the static nature of 3D printed structures, which allows active control of the configuration and function of printed structures. The advantages of 4D printed SMP in the biomedical field are listed below [20, 72–74, 184].

The combination of multifunctional SMP and programmable deformation design, as well as remote controllable actuation methods (e.g. magnetic field and light), enable 4D printed biomedical devices to not only have patient-customized configurations, but also obtain enhanced functionality and adaptive deployment in a remotely controllable manner.

(1) Active control of configuration/performance and personalized customization. To address the challenges of limited designability and reconfigurability in the mechanical properties of metamaterials, Xin drew inspiration from the microscopic architecture of collagen fibers and developed a 4D-printed metamaterial featuring wavy biomimetic ligaments. By adjusting the geometric parameters of the biomimetic ligament, the mechanical properties of the metamaterial can be adjusted over a wide range. More importantly, 4D-printed metamaterials can match the non-linear mechanical responses of specific tissues/organs, and

can be switched between two different biological materials through the SME, providing an effective approach for customizing the geometric configuration and mechanical properties of tissue scaffolds [185]. To further enhance the design flexibility of metamaterials, an active phase SMP and a passive phase TPE were introduced, and a dual-phase composite chiral metamaterial (TPE@PLA-SMP) was designed and fabricated using FDM dual-material 4D printing technology. By adjusting geometric parameters, material compositions, and spatial distributions, the adjustable domain of the 4D SMP metamaterial's mechanical performance was improved, enabling personalized customization of its mechanical properties. Under thermal stimulation, the programmability and reconfigurability of the geometric structure and mechanical properties of the metamaterial were verified. When the TPE was distributed at 0° and 45°, the TPE@PLA-SMP exhibited J-shaped stress–strain behavior similar to that of biological tissues such as skin. Based on the TPE@PLA-SMP metamaterial, a flexible sensor was developed, which enabled monitoring of human movement while cooperating with biological tissues in deforming together [186].

(2) Adaptive and remotely controllable deployment. The shape memory material PGDA with excellent printing and shape memory properties was reported, and the 4D printing PGDA vascular stent was prepared. PGDA had a shape memory transition temperature close to the physiological temperature, and 4D-printed PGDA vascular stents can self-adaptively deploy at body temperature [79]. By incorporating photo- or magneto-responsive materials into the

SMP matrix, non-contact actuated tissue scaffolds can be developed, facilitating remotely controlled deployment, particularly advantageous in anatomically complex regions within the body.

(3) Minimally invasive implantation. Liu *et al* developed a biocompatible, thermoresponsive, amphiphilic dynamic thermoset PU (DTPU) 4D-printed tissue scaffold based on FDM multi-material printing technology, capable of transitioning from 1D to 2D and subsequently to 3D configurations. The DTPU tissue scaffold exhibited temperature-triggered shape memory and water-responsive programmable deformation characteristics, it was in a 2D structural state after printing. The DTPU scaffold can be programmed into a 1D temporary configuration utilizing the SME, facilitating minimally invasive delivery. In a 37 °C aqueous environment, the 4D-printed DTPU scaffold reverted to a 2D configuration based on the SME. Subsequently, it absorbed water and underwent programmed deformation into a 3D structure, thereby providing therapeutic functions for cavity filling and support (figure 7) [187].

(4) Versatility. Researchers have employed 4D-printed SMP in the development of various multifunctional devices, including electronic devices, enabling these devices to possess not only programmable deformation characteristics but also integrated sensing and perception functionalities. Due to the advantage of SMP intelligent structures being able to adaptively change their structural performance/function in response to external stimuli, Li *et al* proposed an autonomous powered e-skin integrating multimodal fusion perception capability and shape memory reconfigurability. The 4D-printed smart hyperelastic scaffold not only had nonlinear mechanical behavior similar to biological tissues, which endowed e-skin with excellent conformal deformation ability; but also realized the flexible transformation of biological tissue mechanical properties through the electro-responsive shape memory property. By monitoring the movements of fingers, wrists, knees, etc in real-time, the e-skin's high sensitivity was verified, showing its potential for application in human movement detection [188]. Furthermore, a multifunctional pressure sensor (4DPS) with adjustable sensitivity and range, featuring a unique coplanar design, was successfully fabricated using nanoparticle-reinforced PLA (CB/PLA) and dual-material extrusion 4D printing technology. Through the SME, the 4DPS can be programmed to adopt various temporary configurations, thereby changing the height and spacing of the electrodes and achieving self-regulating functions for the sensor's monitoring range and sensitivity. Furthermore, the CB/PLA electro-responsive shape-memory behavior endows 4DPS with adaptive deformation characteristics, which has great advantages in monitoring the movements of various complex joints in the human body [189].

Based on the above advantages, 4D printed SMPs have demonstrated attractive competitiveness in biomedical fields such as bone scaffolds, tracheal stents, cardiovascular
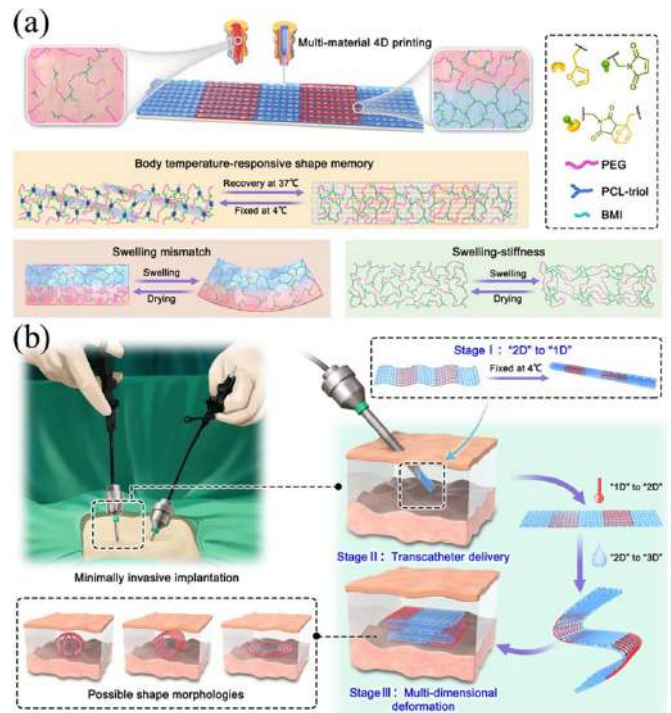

Figure 7. (a) Preparation of multi-material 4D printed DTPU 2D scaffolds. (b) Multidimensional deformation and minimally invasive implantation operation of DTPU scaffolds under temperature and water stimuli. Reproduced from [187]. CC BY 4.0.

devices, drug delivery devices, cell morphology regulation, etc [13, 25, 73, 84, 104, 184, 190, 191].

4.1. Bone scaffolds

Millions of bone repair and reconstruction procedures are performed worldwide each year at an annual cost of billions of dollars. Bone grafting is the gold standard for the treatment of bone defects, but problems such as the limited number of donors and immune rejection cannot be ignored. In addition, the difficulty of precisely matching bone grafts to the contours of bone defects exacerbates the risk of bone nonunion [192]. Implantation of bone scaffolds has become a promising direction of bone defect treatment, especially the programmable bone scaffolds that can adaptively match the contour of bone defect and can be minimally invasive implanted have received increasing attention.

For bone defects, bone scaffolds with suitable pores and internal interconnectivity facilitate cell adhesion and nutrient transfer. Pores of several microns to tens of microns promote cell proliferation and signal transmission, while pores of several hundred microns contribute to angiogenesis, tissue regeneration, extracellular matrix aggregation, etc. Multi-scale porous shape memory PLMC-based bioactive scaffolds were prepared by combining 3D printing and Pickering emulsion template strategies (figure 8), where macroporosity was obtained by 3D printing structural design and microporosity was obtained by freeze-drying Pickering emulsion templates. m-HAp and m-SiO$_2$
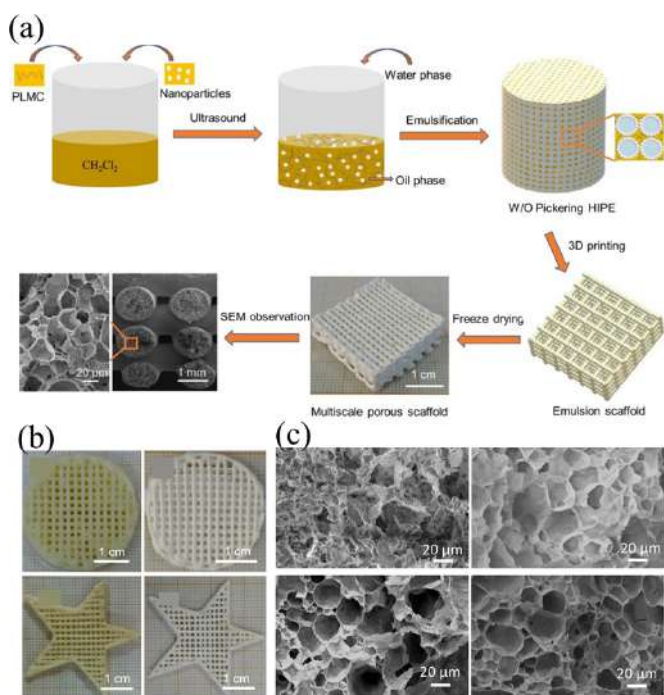
Figure 8. (a) Schematic of multi-scale porous scaffold fabricated by freeze-drying 3D printed Pickering HIPE templates. (b) Physical images and (c) scanning electron microscopy (SEM) images of porous scaffolds. Reproduced from [193], with permission from Springer Nature.

nanoparticles were introduced into Pickering HIPE templates to increase printability and promote scaffold biomineralization capability. The scaffold achieved the sustained release of antimicrobial drugs and showed high shape recovery (10 s). Besides, it promoted cell growth, proliferation, and osteogenic differentiation [193].

Previous work has shown that modulation of SMP surface microstructure can promote bone repair. A 4D printed bilayer morphing membrane consisting of a hydrogel layer and a microstructured SMP layer was prepared (figures 9(a) and (b)), in which the hydrogel layer was programmed to obtain a macrostructure matching the shape of the bone defect, and the SMP layer was actively controlled by external heat to switch the surface microstructure on demand. It was verified by cellular experiments that the smooth SMP layer surface contributed to the adhesion and proliferation of osteoblasts, while the microstructured SMP layer surface can promote cell differentiation. *In vivo* implantation experiments showed that 4D printed bilayer microstructured morphing membranes promoted new bone formation by 30% compared to static membranes [66]. In addition, PPF star-shaped polymers with SME were used for tissue engineering and resorbable PPF 4D printed scaffolds were prepared (figures 9(c) and (d)). PPF is an unsaturated polyester that degrades by hydrolysis of ester bonds to non-toxic fumarate and propylene glycol, and the degradation products can be cleared by metabolic processes. The T_g of the star-shaped PPF scaffold was 29 °C–49 °C, which can be controlled by adjusting the polymer structure and post-curing time of the scaffold [74].

By observing and analyzing the microstructure of lotus root and trabecular bone structure, shape memory porous bone scaffolds were designed (figures 10(a) and (b)) [191]. The bioactivity and osteogenesis of porous scaffolds were evaluated. The results showed that the scaffold promoted cell attachment and proliferation and contributed to the expression of osteogenic factors. The compressed porous scaffold could respond to magnetic fields and be successfully deployed, demonstrating advantages in minimally invasive surgery. Figure 10(c) shows the simulation and experimental results of the shape recovery process of porous bone scaffolds. A macroporous 4D printed shape memory bone scaffold was designed. The shape recovery process of the bone scaffold under a magnetic field was demonstrated, which was expected to contribute to minimally invasive implantation (figure 10(d)) [104].

In addition, osteoinduction-promoting components and stimulus-responsive fillers can accelerate bone healing and enable remotely controlled deployment. BP nanosheets and osteogenic peptides were introduced into poly (lactic acid-co-trimethylene carbonate) (P(DLLA-TMC)) to prepare 4D printed shape memory porous bone scaffolds. The bone scaffolds showed hierarchically porous structure, including designed macroscopic structures of macropores, interconnected square pores of 360 ± 40 μm and micro-pores of 5–20 μm on the rough surface of the scaffold. BP as a biocompatible photosensitive material can absorb NIR light energy into thermal energy. Under NIR irradiation, the scaffold temperature rose to 45 °C due to the photothermal effect of BP, allowing the scaffold to return from its temporary configuration to its initial configuration. Sustained release of osteogenic peptides was essential to induce bone regeneration, and NIR irradiation can promote the release of osteogenic peptides. With periodic NIR irradiation, the rate of osteogenic peptide release from scaffolds was 1.5 times higher than that of unirradiated scaffolds [194]. Additionally, bone scaffolds embedded with Fe_3O_4 nanoparticles can be remotely actuated through NIR irradiation, thereby conforming to irregular bone defects (figure 11) [86].

NIR-triggered intelligent tissue scaffolds were prepared using 4D printed polybutylene succinate (PBS)/PLA composites (figure 12). After functionalization with GO, the tissue scaffold exhibited excellent photothermal properties and achieved remote controllable, dynamic, and accurate 4D shape transformation under NIR irradiation [184].

To address the challenges associated with commercial ocular implants, such as difficulties in precise shaping, inadequate filling capacity, and extensive surgical incisions, Deng introduced AuNPs and nano HA (nHA) into the TPU matrix to develop a multi-functional AuNPs/nHA/PU (AHP) 4D printing SMP composites with near-body temperature actuation and CT imaging capability. Based on the the multi-functional AHP, a 4D-printed orbital scaffold was designed and fabricated to efficiently address orbital defects while enabling personalized therapeutic interventions for ocular disorders. In vitro experiments showed that the AHP scaffold in compressed state can recover its shape within 8 s. When the scaffold was temporarily flattened and implanted into the eye socket, it can also expand and fit the depression within 32 s, providing a feasible solution for minimally invasive, and personalized filling
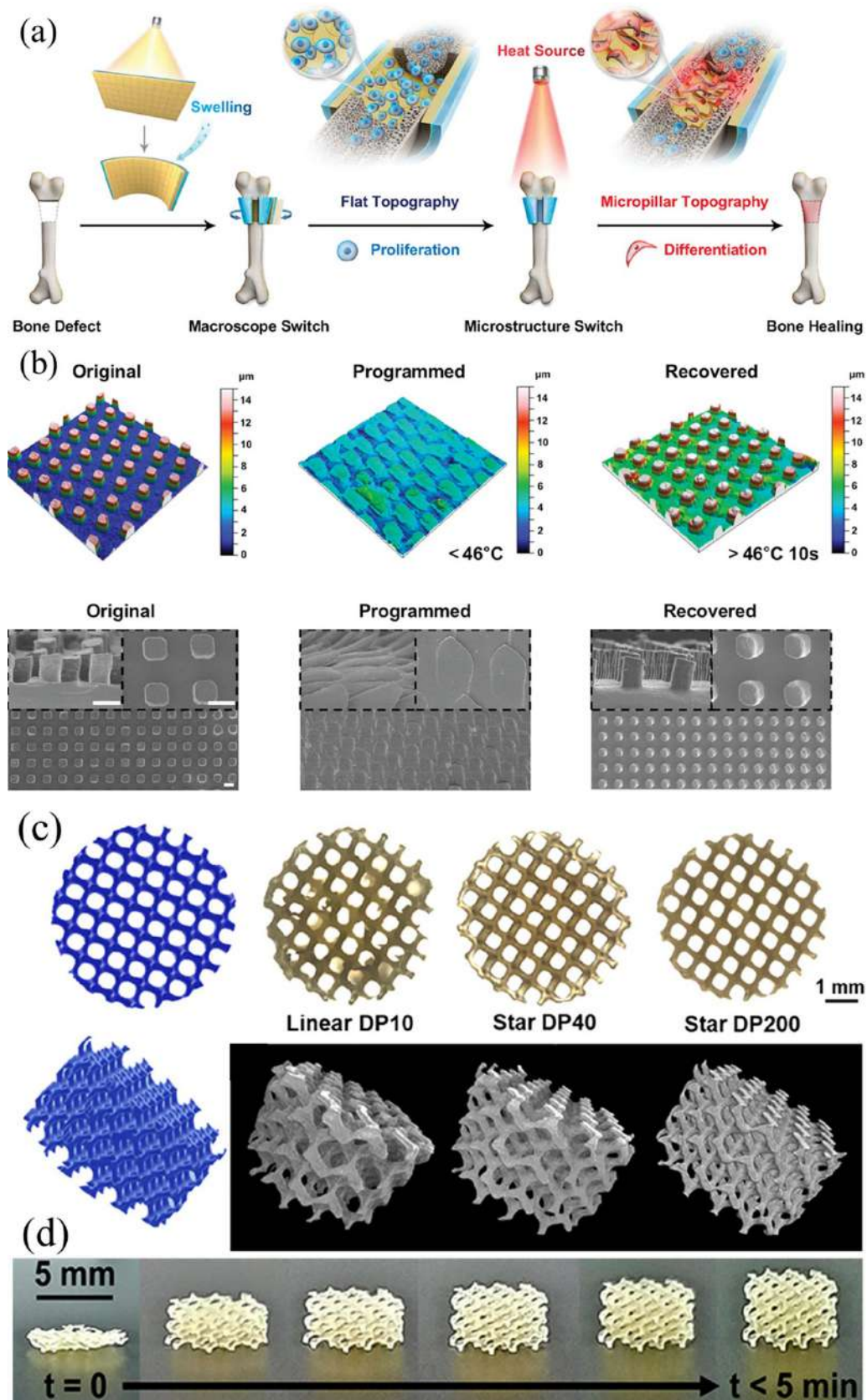
Figure 9. (a) Schematic diagram of the working mechanism of 4D printed bilayer membrane for bone repair. (b) Laser confocal scanning microscopy (LCSM) and SEM images of the shape memory process of the SMP layer. [66] John Wiley & Sons. © 2021 Wiley-VCH GmbH. (c) Scaffold structure created in Matlab using Schoen gyroid triply periodic minimal surface and 4D printed scaffolds prepared from different PPFs. (d) The shape recovery process of PPF scaffold. Reprinted with permission from [74]. Copyright (2020) American Chemical Society.
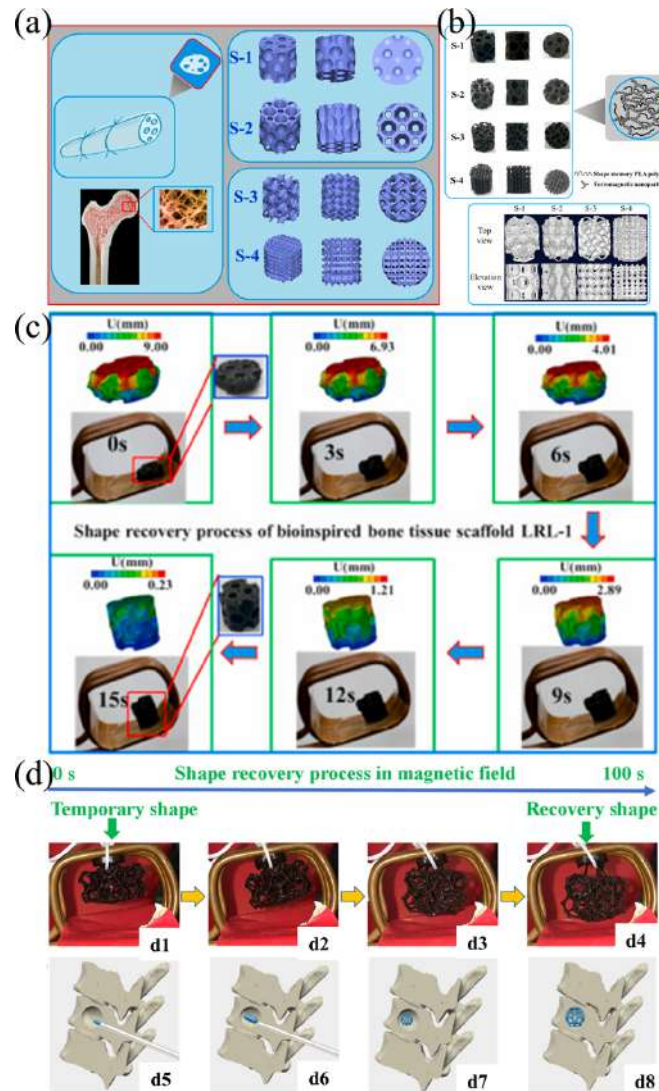
Figure 10. (a) Design and (b) morphological characterization of porous bone scaffolds. (c) Simulation and experimental results of the shape recovery process of S-1 porous bone scaffolds. Reprinted from [191], © 2020 Elsevier Ltd All rights reserved. (d) (d1)–(d4) Shape recovery process of the 4D scaffold under magnetic field and (d5)–(d8) the mechanism of 4D scaffold for bone repair. Reprinted from [104], © 2019 Published by Elsevier Ltd.

of the ocular depression [78]. Besides, by introducing $FeCl_3$-TA-modified MgO nanoparticles into the matrix of SMP, a 4D-printed porous bone scaffold with photo-responsive, antibacterial, and antioxidant properties was designed and prepared. The stent exhibited excellent shape memory properties under NIR irradiation, with the shape recovery process completed within 30 s. Cell experiments showed that the TA-Fe^{3+} chelate not only inhibited bacterial growth but also eliminated free radicals, demonstrating excellent antioxidant properties [195].

4.2. Tracheal stents

The implantation of tracheal stents is an effective treatment for tracheal stenosis and tracheomalacia. Customized 4D printed tracheal stents inject new vitality into the repair of the complex damaged trachea. Personalized endoluminal stents

(e.g. tracheal stents) were printed by SLA using methacrylated PCL with a molecular weight of 10 000 g mol^{-1}, demonstrating the feasibility of low-profile deployment and was expected to reduce the trauma of implantation (figure 13(a)) [20]. Biodegradable PLA-Fe_3O_4 shape memory tracheal stents were investigated. The shape recovery performance of the remotely actuated tracheal stent was evaluated, and the thermal field during the recovery process was monitored [196]. PLA-Fe_3O_4 shape memory biomimetic tracheal stent exhibited excellent shape recovery performance in a magnetic field (figures 13(b)–(d)) [84]. In addition, porous bionic 4D printed shape memory tracheal stents were designed based on a Siliceous venus flower basket for tracheal stenosis (figure 14). The tracheal stents were prepared by SMPU compounded with different contents of cross-linking agents and magnetic nanoparticles. The shape recovery process of the bionic tracheal stents was simulated using the finite element method, and the temporary
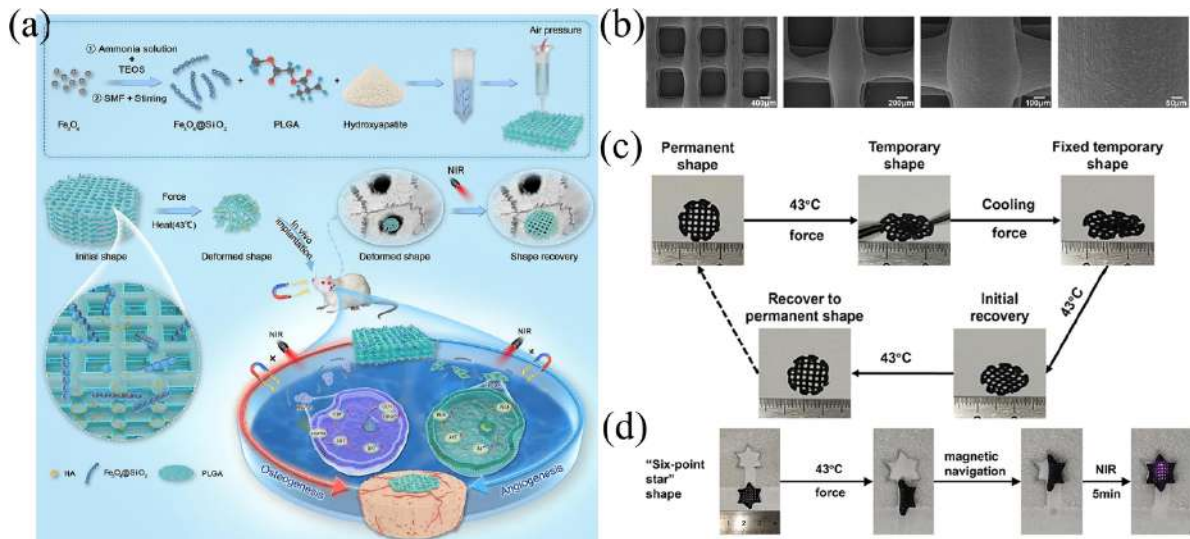
Figure 11. (a) A schematic diagram of NIR stimulation treatment for irregular bone defects. (b) Microstructure of bone scaffold. (c) The shape-memory process of bone scaffold. (d) The magnetic field facilitated the movement of the scaffold, while NIR stimulation enabled the scaffold to effectively fill the irregular defect. Reprinted from [86], © 2024 Elsevier B.V. All rights reserved.

shape of the stent was programmed as an X shape. The simulation results showed that the shape recovery rate of stents was about 95%. In addition, the shape memory deployment behavior of the bionic tracheal stent under a magnetic field was evaluated by folding the stent into a spiral shape, and the stent could complete shape recovery within 20 s due to the presence of magnetic nanoparticles (15 wt.%) [83].

Besides, shape memory biomaterials endowed with photothermal therapeutic functions have been developed, demonstrating the potential for applications in tumor therapy and intraluminal stents (figure 15). Light-actuated shape memory composites (AuNPs/SMPU) were prepared by introducing gold nanoparticles into SMPU, which showed good printability. The cytocompatibility tests showed that AuNPs/SMPU had good biocompatibility, and the cell survival rate was more than 95%. AuNPs/SMPU exhibited an outstanding photothermal effect, and the cell viability of breast cancer cells in contact with it decreased by 80%, achieving locally controlled tumor ablation (figure 15(a)). 4D printed AuNPs/SMPU scaffolds enabled autonomous light-actuated shape recovery and can be adaptively deployed from small-volume temporary shapes to large-volume permanent shapes, demonstrating the potential for remote control and minimally invasive treatment (figures 15(b) and (c)) [197].

4.3. Cardiovascular devices

Applications of 4D printed SMPs in cardiovascular devices include occlusion devices, cardiac patches, and vascular stents [73, 81, 93, 190, 198]. Transcatheter closure is an effective method for the treatment of congenital heart defects (CHD) and stroke-related left atrial appendages (LAA). Atrial septal defect (ASD), a common CHD, is an abnormal hole in the right and left atria that allows for abnormal blood exchange between the right and left atria. The currently commonly used occlusion devices are mainly woven through Nitinol wires

and have the potential hazard of being permanently present in the body due to non-degradability. In addition, problems such as nickel allergy, wear, tear, and embolization have been reported [73, 190].

Personalized, bioabsorbable, and remotely controlled 4D printed shape memory occlusion devices were first designed and fabricated in 2019 (figure 16), which was expected to avoid serious problems such as nickel allergy and late embolism caused by metal occlusion devices [73]. The unique ligament design of the device allowed it to undergo large deformations and the temporary shape can be programmed to a linear temporary shape. Due to the presence of magnetic nanoparticles, the linear temporary shape of the device can recover to the initial double-disc shape under a magnetic field. The biodegradability, biocompatibility, and occluding feasibility were evaluated. Besides, the large mismatch in mechanical properties between the metal occlusion devices and the surrounding tissue may lead to wear and even perforation. Inspired by collagen fibers, 4D printed bioinspired LAA occlusion devices with customizable configurations and mechanical properties were developed (figures 17(a) and (b)) [190]. Through iterative optimization, the bioinspired structure with similar stress–strain behavior to the LAA tissue was obtained, and the cooperative deformation with the LAA tissue was realized to avoid the risk of wear and perforation.

4D printed NIR light-sensitive cardiac patches with tunable curvature and aligned microgroove structures were developed to mimic myocardial tissue at both macroscopic and microscopic scales (figure 17(c)). Human-induced pluripotent stem cell-derived cardiomyocytes (hiPSC-CMs), mesenchymal stem cells (hMSCs), and endothelial cells (hECs) were cultured on patches and cell morphology was analyzed to obtain optimized microgroove widths. After culturing cells on optimized flat patches, the patches underwent dynamic shape changes induced by light, and cells remained evenly distributed on the curved 4D patch (figure 17(d)) [81].
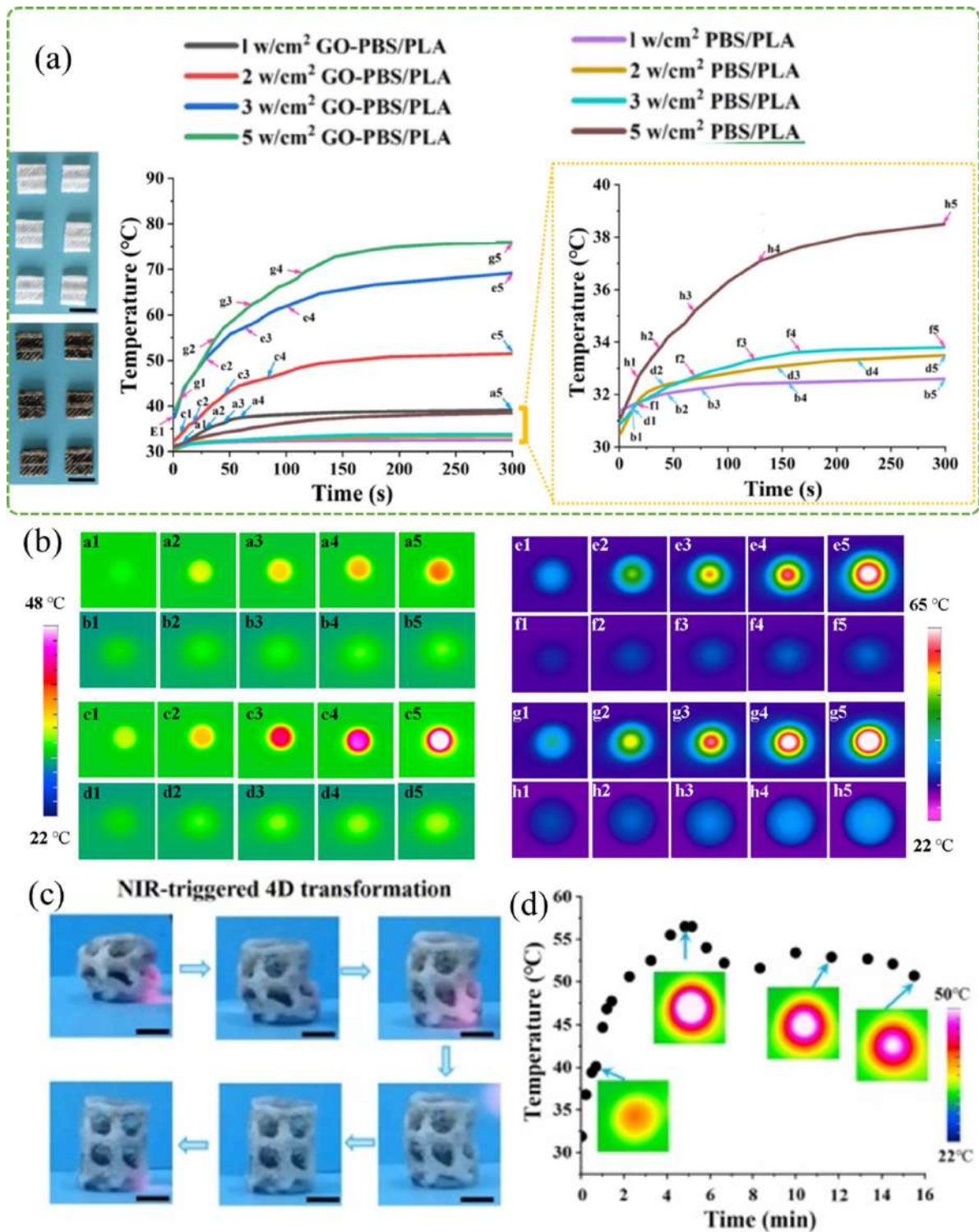
Figure 12. (a) PBS/PLA and GO-PBS/PLA samples, and their temperature changes under NIR irradiation. (b) Infrared thermogram of GO-PBS/PLA and PBS/PLA samples. (c) Shape recovery of the GO-PBS/PLA scaffold. Scale bar: 5 mm. (d) Temperature evolution of the GO-PBS/PLA scaffold during shape recovery. Reprinted from [184], © 2021 Elsevier Ltd All rights reserved.

4D printed SMPs also show potential application in vascular stents, which are mainly used to restore the lumen in the treatment of vascular stenosis caused by atherosclerosis. 4D printed shape memory vascular stents were designed based on the negative Poisson's ratio structure optimized by genetic algorithm (figures 18(a) and (b)). Stress distribution

of the vascular stents during shape recovery was obtained by the finite element method. The experimental results showed the excellent shape memory behavior of the stent and its ability to rapidly open the simulated stenotic vessel [93]. Besides, based on DIW printing technology and ultraviolet-cross-linked PLA magnetic nanocomposite inks, 4D active
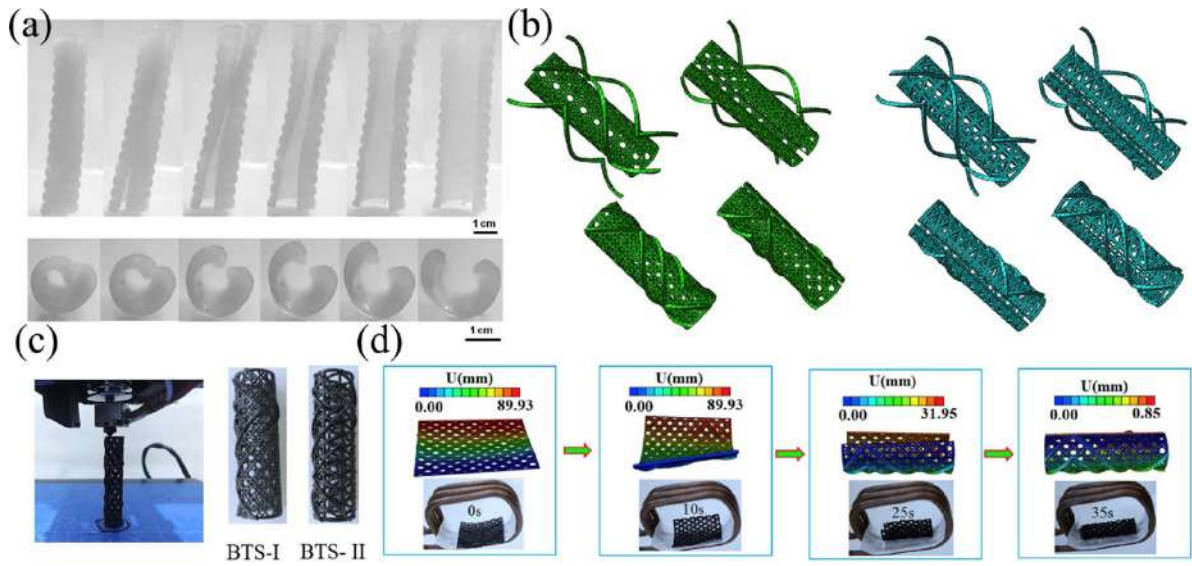
Figure 13. (a) Macroscopic shape memory behavior of personalized endoluminal stents. [20] John Wiley & Sons. © 2016 WILEY-VCH Verlag GmbH & Co. KGaA, Weinheim. (b)–(d) Biomimetic tracheal stent. (b) Schematic diagram of biomimetic tracheal stents. (c) Printing of biomimetic tracheal stents. (d) The shape recovery process of biomimetic tracheal stent under magnetic field stimulation. Reprinted from [84], © 2019 Elsevier Ltd All rights reserved.
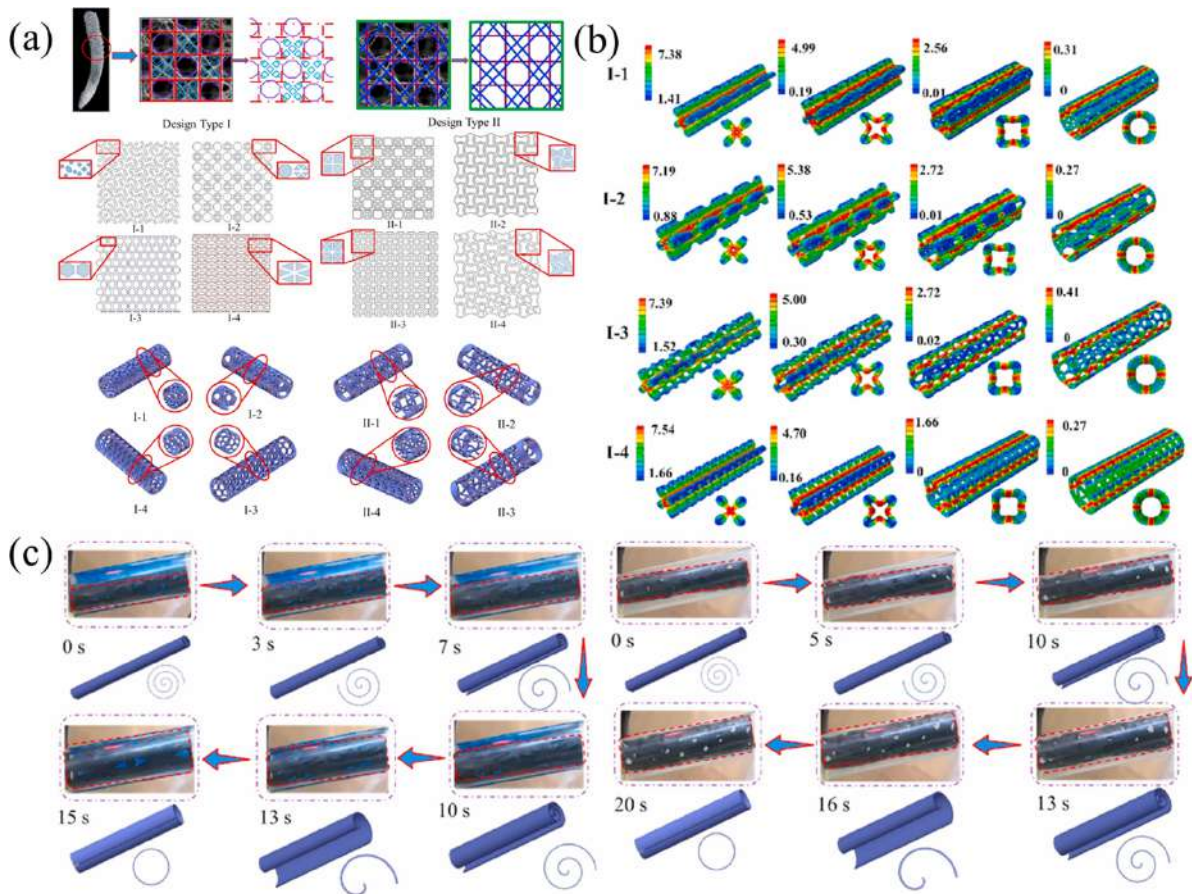

Figure 14. (a) Structural design of 4D printed bionic tracheal stents based on siliceous Venus flower basket. (b) Simulation of shape recovery of 4D printed bionic tracheal stents. (c) Deployment of 4D printed bionic tracheal stents under alternating magnetic field. Reprinted from [83], © 2022 Elsevier Ltd All rights reserved.
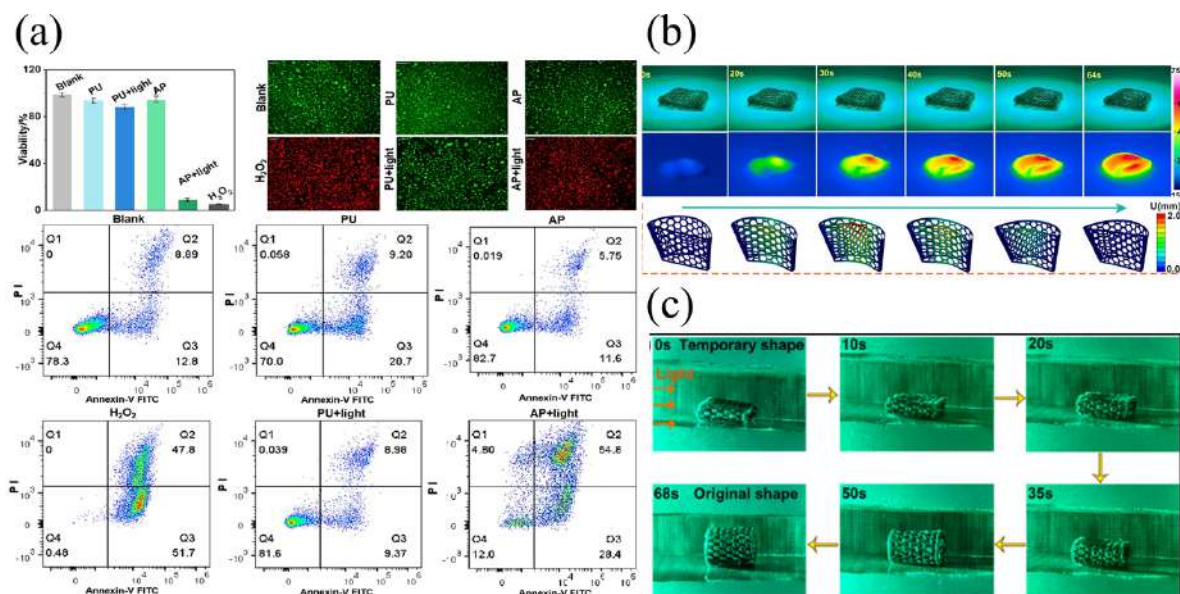
Figure 15. Light-actuated shape memory AuNPs/SMPU. (a) Viability of cancer cells after different treatments (blank, PU, PU + light, AP, AP + light, and H_2O_2). (b) Experimental and simulated light-actuated shape recovery process of tissue scaffolds. (c) Light-actuated shape recovery process of the 4D printed intraluminal stent. Reprinted with permission from [197]. Copyright (2022) American Chemical Society.

shape-changing structures with thermal and remote actuation behavior were printed (figures 18(c) and (d)) [114]. The cross-linked printed structures showed high shape fixation and shape recovery rates, and the potential application of printed helical structures in vascular stents was demonstrated.

4.4. Active regulation of cell morphology

The active deformation behavior of 4D printed shape memory structures allows for active dynamic control of cellular morphology, enabling highly site-specific tissue or organ mimicry. For example, cells were cultured on 4D printed scaffolds, and mechanical strain stimulus was transferred to cells when the scaffold underwent controlled time-dependent shape changes [82]. Self-morphing cell culture substrates are crucial in the process of cell differentiation, markedly promoting cellular differentiation (figure 19) [80]. Cells on 4D printed scaffolds became more elongated after the scaffold underwent a change from a temporary shape to its permanent shape. The design of an SMP surface micropattern can guide the cells to grow in a specific direction, and the cells can be highly aligned along the micropattern to form an uninterrupted cell sheet [199].

Scroll-like scaffolds with anisotropic internal morphology were prepared, which were also capable of guiding the directional alignment of cells (figure 20). Through 3D printing of methacrylated alginate (AA-MA) and melt electrowritten shape memory PCL fibers, AA-MA/PCL bilayer scaffolds with programmable surface patterns and active shape-changing capability were obtained. The patterned surface generated by the shape-memory PCL fibers ensured highly oriented cellular arrangement, which could not be achieved by the single AA-MA scaffold. Moreover, myoblasts cultured inside

the scaffold showed high cell viability. The fabricated scaffolds were expected to be used for tissue engineering with uniaxially oriented cells, such as skeletal muscle, heart, and neural tissues [85].

4.5. Drug delivery devices

Due to programmable and reconfigurable characteristics, 4D printed SMPs contribute to the development of intelligent drug delivery devices. PVA-based intravesical drug delivery retention devices were prepared by 4D printing. PVA enabled programmable deformation to facilitate drug delivery and a large number of hydroxyl groups in the PVA side chains allowed its dissolution in water, avoiding secondary removal of the device. The printed samples were able to recover to their original shape under water stimulus, accompanied by controlled release of the tracer. The results tentatively demonstrated the effectiveness of the intravesical drug delivery retention device [156].

By designing the molecular structure of SMP, new drug-loading sites can be developed. Tissue-engineered biomaterials suitable for deployable biomedical devices (DMDs) were developed based on photocrosslinked PCL (figure 21). β-cyclodextrin (β-CD) was used as an initiator for ring-opening polymerization of caprolactone, and 21-armed star polymers with methacrylated end-group were synthesized. The excellent biocompatibility of the developed DMD materials was demonstrated by cell proliferation, hemolysis, and subcutaneous implantation tests. The shape memory fixation and recovery rates of DMD materials were both above 98%. In addition, the feasibility of drug loading of DMD materials was verified with everolimus as a representative drug. The
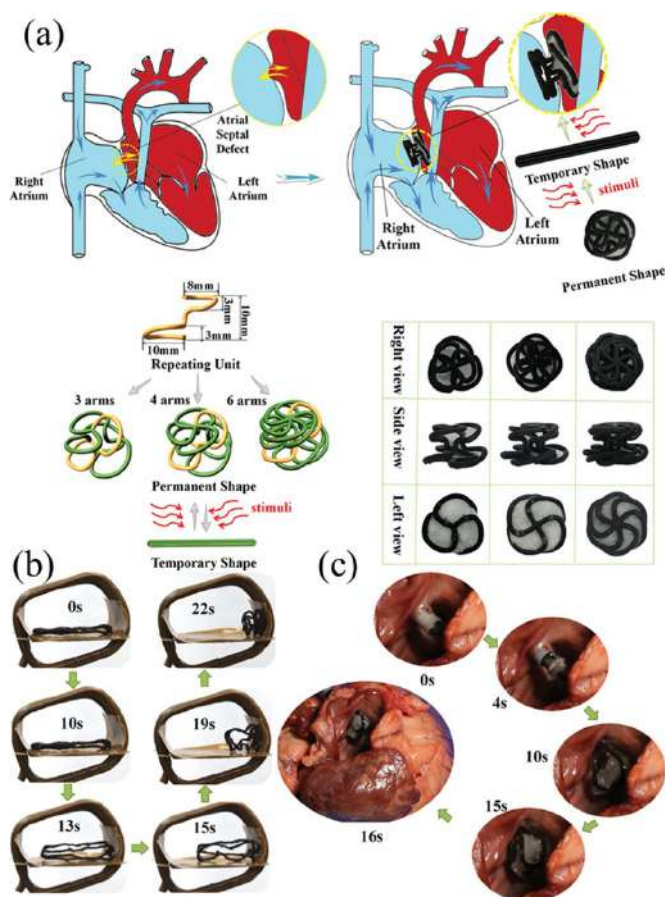
Figure 16. (a) Occluding process of 4D printed shape memory ASD occlusion devices and structure of the devices. (b) The shape recovery process of the 4D printed ASD occlusion devices. (c) In vitro occlusion tests of the device. [73] John Wiley & Sons. © 2019 WILEY-VCH Verlag GmbH & Co. KGaA, Weinheim.

β-CD as a star-shaped polymer core provided a hydrophobic core for drug loading and could act as a drug loading site for everolimus. The cumulative release of everolimus within 42 d was 43%. The everolimus-loaded DMD material was able to inhibit hEC proliferation and reduce the risk of thrombosis in vascular stents [2]. Besides, a series of thermoresponsive 4D printed composite materials were synthesized based on varying compositions of PLA and PCL, facilitating controlled and sequential actuation. The sample can recover its original state within 1.2 s, and the shape fixity/recovery rate was all above 92%, showing excellent shape recovery performance. Furthermore, the effect of the PLA/PCL samples loaded with different colored particles in the process of sequential drug release was demonstrated: the sample in the temporary shape first wrapped the drug particles, followed by the green particles releasing in 0.5 s under stimulation, the blue particles releasing in 1 s, and the red particles releasing in 6 s in the last, verifying the feasibility of the PLA/PCL composite in the field of drug release (figure 22(a)) [200]. In addition, by blending different hydroxyl-containing monomers and introducing different concentrations of magnetic nanoparticles Fe_3O_4, Anand *et al* prepared a dual-component magnetically responsive shape-memory PU. The cell proliferation

and drug release experiments showed that the drug release rate can be controlled by changing the molecular structure of the polymer and the concentration of the nanoparticles. Low-particle-concentration highly cross-linked networks reduced the drug release concentration, while high-concentration linear networks promoted drug release. In alternating magnetic fields, the magnetothermal effect can accelerate the release of drugs. Compared to the initial configuration, the temporary configuration of the sample resulted in an increased cross-linking density of molecular chains, which impeded the drug release process. Thus, by modulating the crosslinking network and particle concentration of the polymer, remote precise triggering and sustained release of single or multiple drugs under alternating magnetic fields can be effectively achieved [201]. Furthermore, the dynamic changeable microstructure provides the possibility of reducing the size of drug targeted delivery and release devices. Shape-memory microcapsules offered the benefits of straightforward preparation and programmable morphology, while simultaneously demonstrating outstanding shape-memory characteristics (figure 22(b)) [202].

4.6. Others

Other biological applications of 4D printed SMPs include soft tissue repair, cell culture devices, wearable devices, etc 4D printed polycarbonate resin ink was developed for soft tissue repair (figure 23). The T_g of the resin can be adjusted between $-20\ ^\circ$C and $80\ ^\circ$C due to the adjustable ratio of carbonate monomers and the presence of PU bond. Scaffolds with complex geometry were printed through photopolymerization, capable of shape recovery at body temperature. Polycarbonate was degraded through surface erosion, which can reduce the risk of premature failure of the scaffold. The degradation products were nonacidic, avoiding inflammatory reactions that may be caused by an acidic environment. The cytocompatibility of the scaffold was assessed by contact with different cells. Different cells proliferated throughout the scaffold and no statistical differences were seen, indicating that the scaffold was cytocompatible. *In vivo* implantation experiments showed that adipocyte lobules adhered to the surface-eroding scaffold within 2 months and neovascularization was observed. The scaffold had the advantages of excellent printability, shape recovery performance, surface erosion degradation, and biocompatibility, showing promising potential in the repair of cardiovascular, kidney, and other soft tissues [203].

4D printed SMP structures show great potential in the next generation of cell culture devices. 4D printed transformable tube arrays (TTAs) were prepared using PμSL based on temperature-responsive SMPs (figure 24). The TTA allowed direct transfer of large-scale 3D culture models from well plates to small histology cassettes, enabling parallel culture and tissue analysis. After printing, post-processing procedures were performed to allow complete cross-linking of the SMP and removal of residual cytotoxic material. The 4D printed TTA can be programmed to 3.6 times its original size to match the size of histology cassettes and 96-well plates. By eliminating the need for collection, transfer, and repeat sectioning of
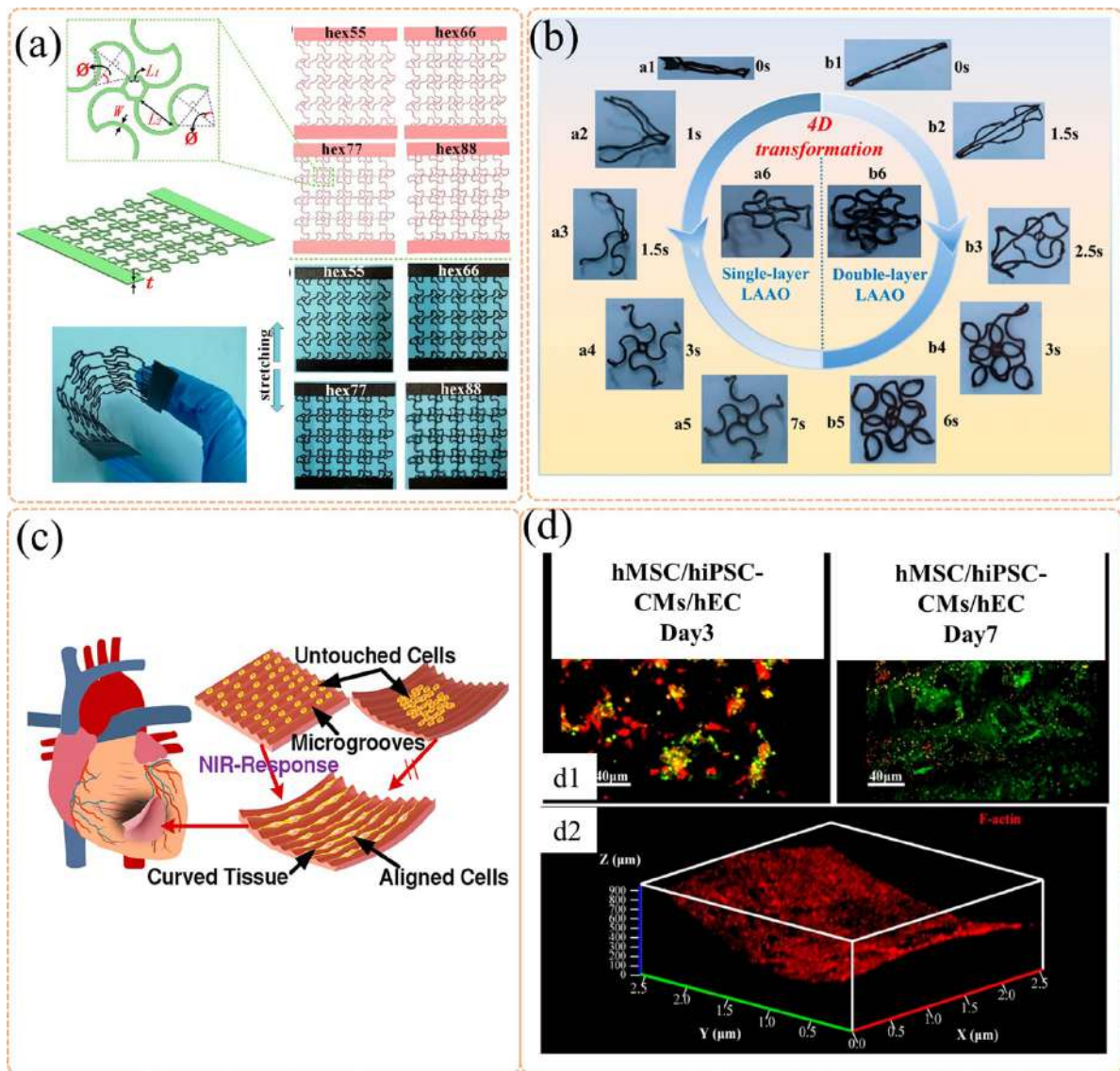
Figure 17. (a) Design of bioinspired structure. (b) The 4D transformation process of LAA devices. Reprinted with permission from [190]. Copyright (2021) American Chemical Society. (c) Design of 4D printed cardiac patch. (d) (d1) Immunofluorescence staining images of three cells (hMSCs, hECs, and hiPSC-CMs) co-cultured on 4D cardiac constructs. (d2) F-actin staining of cells on the surface of the 4D construct after deformation. Reprinted with permission from [81]. Copyright (2021) American Chemical Society.

a single specimen, the TTA can reduce the histological processing time for bulk 3D culture analysis by an order of magnitude. High-throughput analysis of TTA-enabled 3D cultures may help advance innovations in 3D culture applications, such as disease modeling and drug development [72].

Wearable devices refer to devices that can come into contact with the human body, monitor and record physiological parameters, and provide diagnostic, preventive, and other functions, characterized by their wearable and intelligent features. 4D-printed SMPs exhibit strong adaptability and high conformability, enhancing the sensitivity of electronic devices and demonstrating significant potential in emerging wearable technologies. Based on the FDM 4D printing technology and the spider-inspired slit structure, a self-adaptive multi-functional wearable electronic device with sensing and actuation capabilities was developed (figure 25).

Upon exposure to infrared light stimulation, the geometric configuration of the device's microscopic slits underwent a progressive transformation from a trapezoidal structure to an inverted trapezoidal structure, enabling self-adaptive morphological transformations. The device achieved a integration of sensing and actuation functionalities, facilitating precise identification of thermal and mechanical signals. By testing human movements and physiological signals, the device demonstrated its feasibility in the field of health monitoring [204]. Inspired by the superhydrophobic microstructures on lotus leaves, a columnar microstructure surface SMP electrode film was designed. Combined with 4D printing fractal metamaterial frameworks, a multi-layer structure flexible shape-memory electronic device was prepared, with reconfigurability, high sensitivity, and high adaptability to the detection site. Compared to flat electrodes, the multifunctional
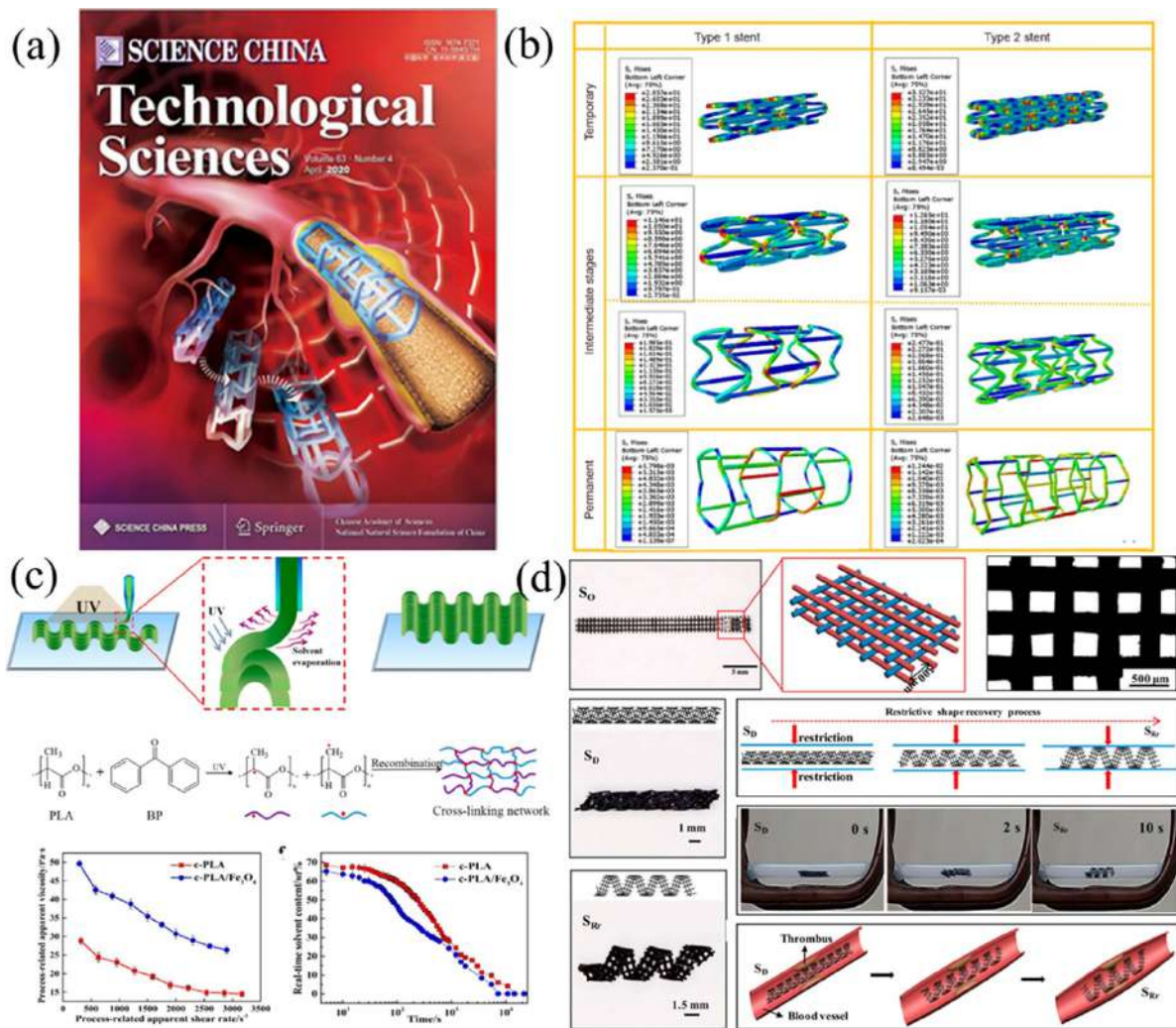
Figure 18. (a) Schematic diagram of 4D printed negative Poisson's ratio vascular stent reopening the stenotic vessel. (b) Simulation of the shape recovery process of two negative Poisson's ratio vascular stents. Reproduced from [93], with permission from Springer Nature. (c) Schematic diagram of the printing process of 4D active shape-changing structures and the characterization of ink properties [114]. (d) 4D printed vascular stent and its shape recovery process. Reprinted with permission from [114]. Copyright (2016) American Chemical Society.

electronic device achieved a significant improvement in signal-to-noise ratio and sensitivity, with a 10-fold and 4-fold increase, respectively. Furthermore, the stimulus-responsive properties of fractal metamaterials align with the nonlinear stress–strain behavior of tissues, providing the possibility of adaptively matching the mechanical properties of tissues, skin, and organs, with broad application prospects in areas such as implantable medical devices and wearable electronic devices [205].

PLMC: poly(D,L-lactide-co-trimethylene carbonate); TCP: tricalcium phosphate; P(DLLA-TMC): poly(lactic acid-co-trimethylene carbonate); PCLDA: PCL-diacrylate; PBS: poly(butylene succinate); BPO: benzoyl peroxide; SMPU: shape memory polyurethane; AuNPs: gold nanoparticles; SOEA: soybean oil epoxidized acrylate; PU: polyurethane; AA-MA: methacrylated alginate; PVA: polyvinyl alcohol; GLY: glycerol; β-CD: β-cyclodextrin; BPA: bisphenol A ethoxylate dimethacrylate.

5. Conclusion

In conclusion, in the paper, the deformation mechanism of SMP is described, the SMP actuated by different actuation methods and their limitations are elucidated, and promising actuation methods are pointed out for applications in the biological field. The realization methods of 4D printing, such as FDM, DIW, DLP, etc, are reviewed, and the advantages and disadvantages of different printing methods are summarized. The advantages of 4D printing SMP in biomedical applications are highlighted, and the applications of 4D printing SMP in bone tissue, tracheal scaffolds, cardiovascular scaffolds, and drug delivery are reviewed.

4D printing inherits the advantages of 3D printing in fabricating complex configurations with precision and adds the ability for structures to be dynamically and actively controllable in time and space, making it a game changer for smart medical devices. However, the widespread application of 4D
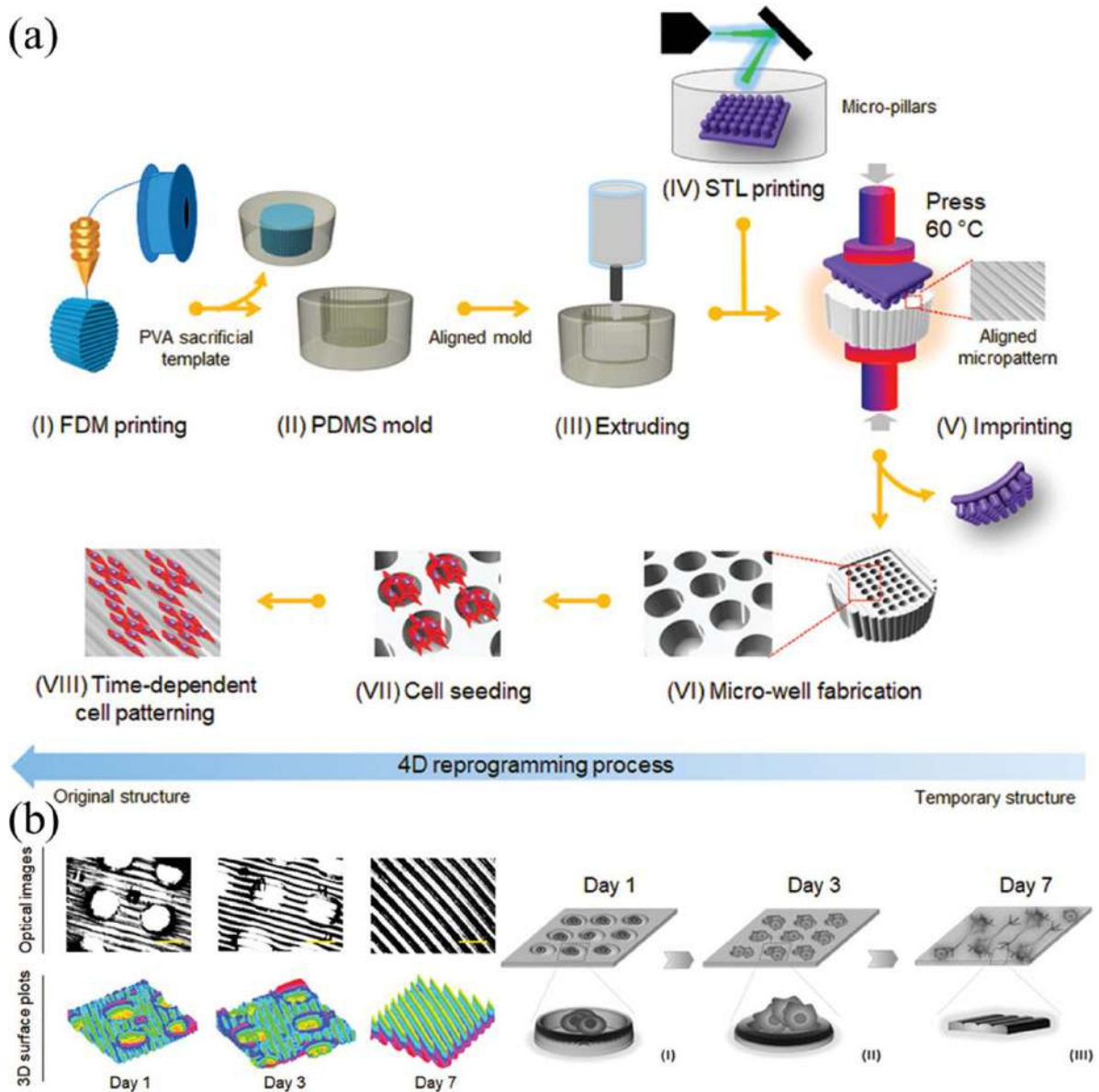
Figure 19. (a) A self-transforming cell culture substrate. (b) The transformation process of the shape memory cell culture substrate and the corresponding changes in cells. Reproduced from [80]. CC BY 4.0.

printed SMP medical devices still faces many challenges and still requires much effort.

6. Future perspective section

In the future, research on 4D printed SMP biomedical devices can be carried out from the following aspects.

(1) Significant effort is required to develop novel 4D-printed SMP biomaterials. For 4D printing SMP materials used in the biomedical field, especially when used for in-body implants, it is essential that the temperature at which shape memory transformation occurs aligns closely with

the physiological temperature. Therefore, under physiological conditions *in vivo*, precise regulation of the shape recovery temperature and the assurance of a rapid shape recovery rate are crucial. Currently, the majority of 4D-printed SMPs are 1W SMPs that lack the capability for reversible shape transformations. This limitation poses significant challenges for the reuse of 4D-printed biomedical devices, as each instance of reapplication necessitates manual reshaping. Furthermore, 4D-printed multiple SMPs are also worth studying, thus endowing 4D-printed implant devices with multiple SMEs. For instance, in the domain of tissue scaffolds, multi-shape 4D-printed scaffolds possessing multiple SMEs can adopt distinct configurations at various stages of tissue repair. This
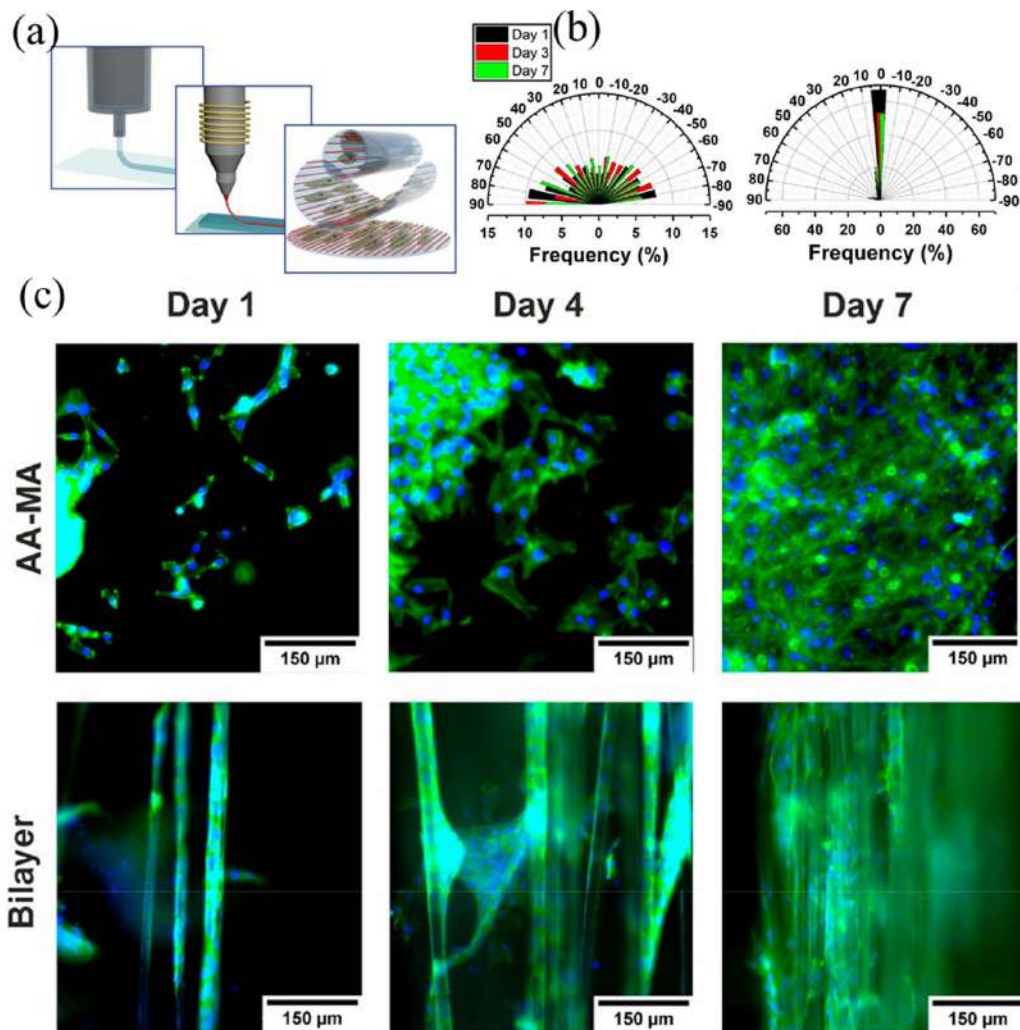
Figure 20. (a) Preparation of AA-MA/PCL bilayers. (b) Frequency distribution of cell alignment in AA-MA (left) and bilayers (right). (c) Staining of cells cultured on AA-MA and AA-MA/PCL bilayers. Reprinted with permission from [85]. Copyright (2021) American Chemical Society.

intrinsic adaptability allows them to respond optimally to the specific physiological conditions encountered at each stage, thereby promoting and accelerating the healing process.

Non-contact actuation techniques, including light- and magnetic- actuation, are essential for biomedical devices, particularly in facilitating access to difficult-to-reach anatomical regions within the body. However, the current non-contact-driven 4D printing SMPs mainly rely on adding functional fillers, such as magnetically sensitive/photosensitive particles. The development of 4D printing SMP materials with inherent responsive properties could further facilitate accurate response to external stimuli, improve printing accuracy, and reduce the impact of fillers on mechanical properties.

Therefore, in general, 4D printing SMP biomaterials are very limited, and there is a need to broaden the scope of 4D

printing SMP biomaterials. The establishment of a comprehensive library of printing materials is the prerequisite and cornerstone for the in-depth development of 4D printing technology in the biomedical field.

(2) The manufacturing of 4D printed SMP structures lacks theoretical guidance. There is no theoretical support for the regulation of the printing parameters during the printing process of the structure, the mechanism of the influence of the printing parameters on the 4D printing manufacturing defects (e.g. interfaces between the printed layers, micropores, microcracks) is not clear, and there is no precise correlation model for the relationship between the printing parameters and the performance of the structure. In the future, the influence of printing parameters on the defects of 4D printed structures can be deeply investigated, and the characteristics and distribution laws of defects can be
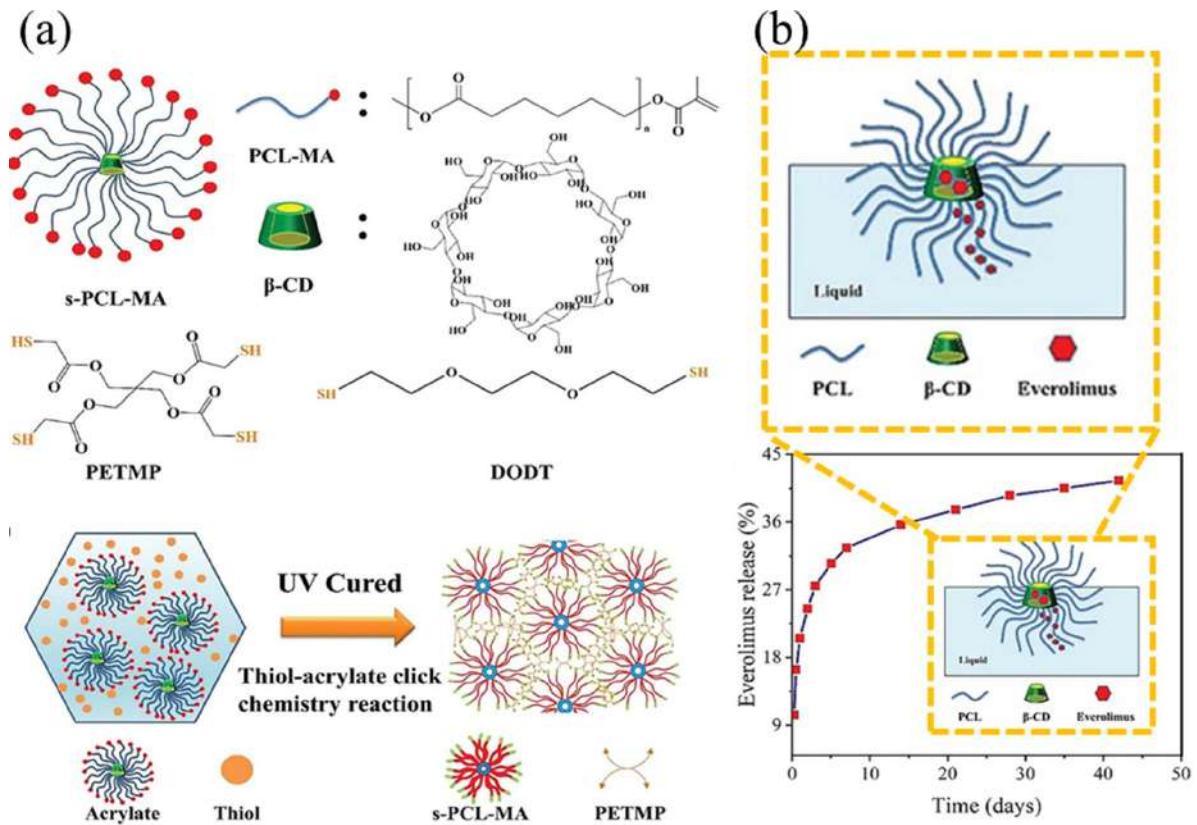
Figure 21. (a) Synthetic schematic of DBD materials (xsy-PCL). (b) Drug release profile and drug delivery mechanism (enlarged view) of DMD material loaded with everolimus. [2] John Wiley & Sons. © 2022 Wiley-VCH GmbH.
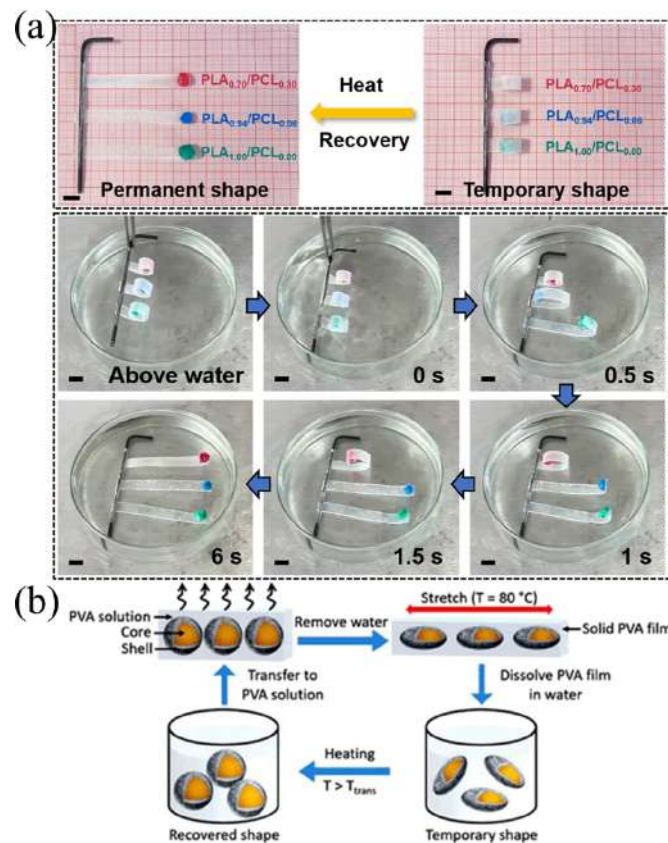

Figure 22. (a) Simulated drug sequential release process. Reproduced from [200], with permission from Springer Nature. (b) Micro-capsules with active shape-shifting properties. Reprinted with permission from [202]. Copyright (2020) American Chemical Society.
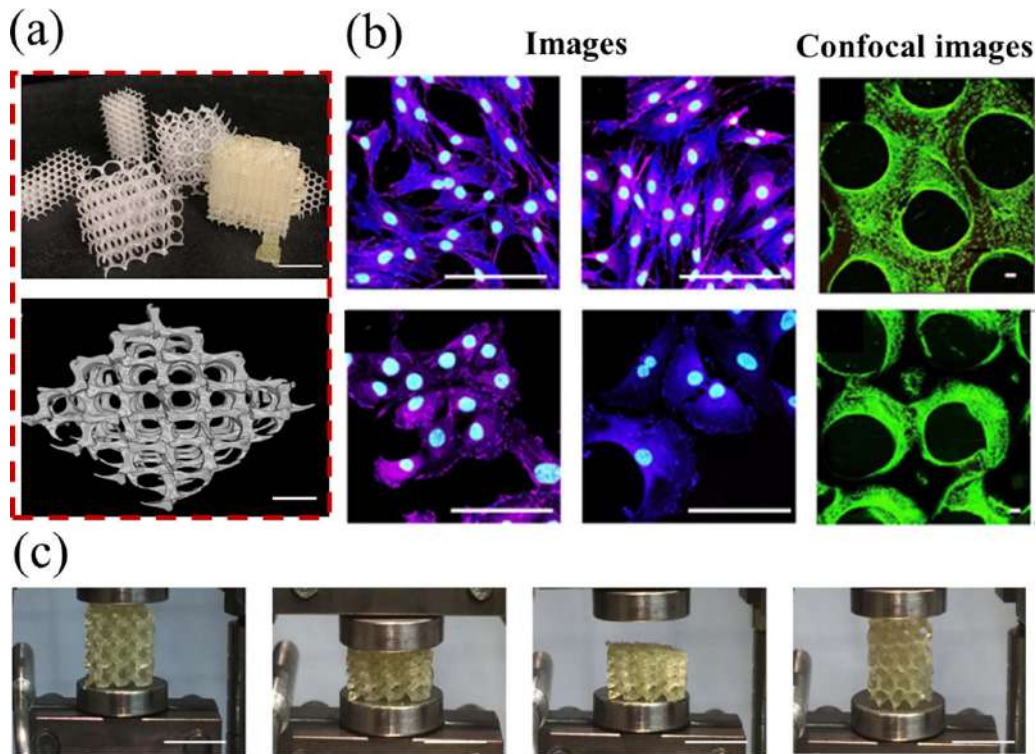
Figure 23. (a) Prototype and micro-CT image of the 4D printed scaffolds. Scale bar = 2 mm (upper image), scale bar = 500 μm (lower image). (b) Images of adipocytes and fibroblasts in contact with scaffolds. Scale bar = 500 μm. (c) The shape recovery process of the 4D printed scaffold. Scale bar = 1 cm. Reproduced from [203]. CC BY 4.0.

explored. The formation mechanism of 4D printing defects and the influence of defects on the performance of 4D printed structures can be investigated. The accurate correlation model between printing parameters, defects and properties can be established to realize the accurate construction of 4D printed SMP structures. This will help improve the repeatability and uniformity of preparation of 4D printed structures and help control product quality.

(3) The dynamic deformation process of 4D printed SMP structures lacks theoretical guidance, and it is urgent to develop theoretical models to accurately guide the deformation process. This involves two aspects: first, the programming deformation design of 4D printing SMP lacks theoretical guidance. At present, it mostly relies on empirical programming of application scenarios to design temporary configurations, lacking standardized guidelines and theoretical models. In addition, there is no theoretical support for the dynamic recovery process of the structure, and relevant models need to be developed to accurately control the deformation of the structure.

(4) Personalized manufacturing and programmable deformation are the advantages of 4D printing SMP medical devices, and its practical application cannot be separated from the close cooperation of doctors and engineers.

Doctors obtain the patient's personalized anatomy through CT scanning, and engineers then use 3D reconstruction technology to customize medical devices and prepare personalized medical devices through 4D printing. The high efficiency and low time cost of this entire process are the prerequisites for the wide application of dynamically customized 4D printed SMP medical devices. Therefore, scanning and reconstruction technology, as a basic technology, needs to be improved in accuracy and controllability accordingly.

(5) Low cost and scalable manufacturing are the cornerstones of 4D printed SMP biomedical devices for clinical applications. Some 4D printed SMP biomaterials are integrated with satisfactory functions, but their cumbersome manufacturing process or high cost leads to their scaled-up fabrication and high-throughput production becoming pressing issues in the future. Therefore, a trade-off between the fabrication process, material properties, and production cost is necessary.

(6) The effects of 4D printed SMP active materials on living organisms need to be clarified. For novel 4D printed SMPs, prolonged, high-volume *in vivo* animal experiments are necessary and need to be combined with a high standard of tissue analysis to provide insight into the effects of 4D printed SMPs on tissues.
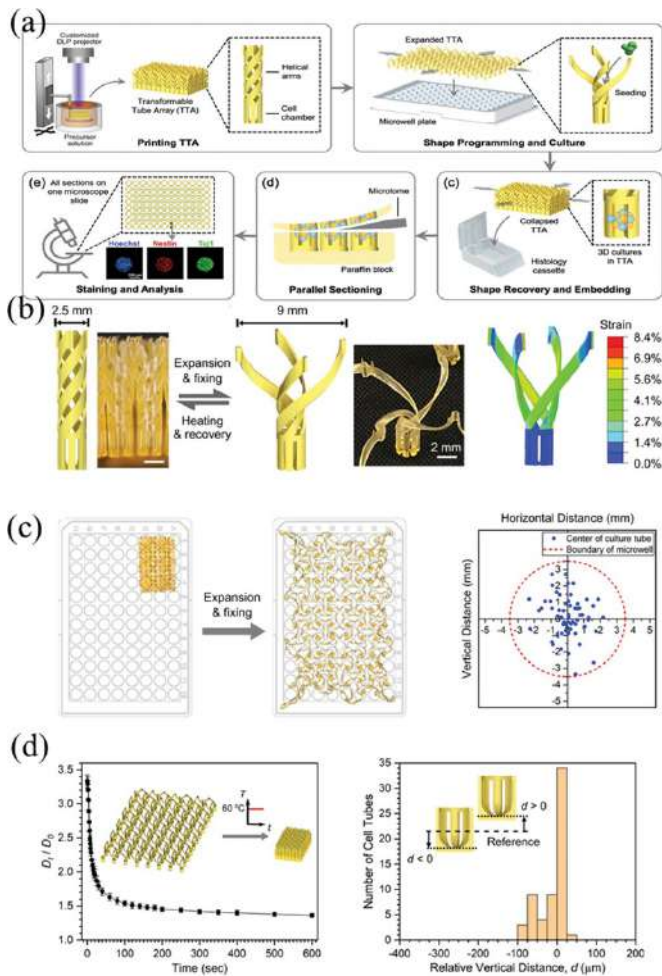
Figure 24. (a) Schematic of 4D printed TTA being used for high throughput cell culture and histological study. (b) The stretched and fixed TTA was matched to a 96-well plate. (c) Culture tubes in folded and expanded states. (d) Shape recovery of the 4D printed TTA. [72] John Wiley & Sons. © 2020 Wiley-VCH GmbH.

(7) The convenience of the 4D printing SMP actuation method needs to be further improved. Combining with artificial intelligence and advanced information technology may contribute to the development of new types of actuation methods.

Further development of 4D printed SMPs requires interdisciplinary efforts to jointly drive the clinical translation of
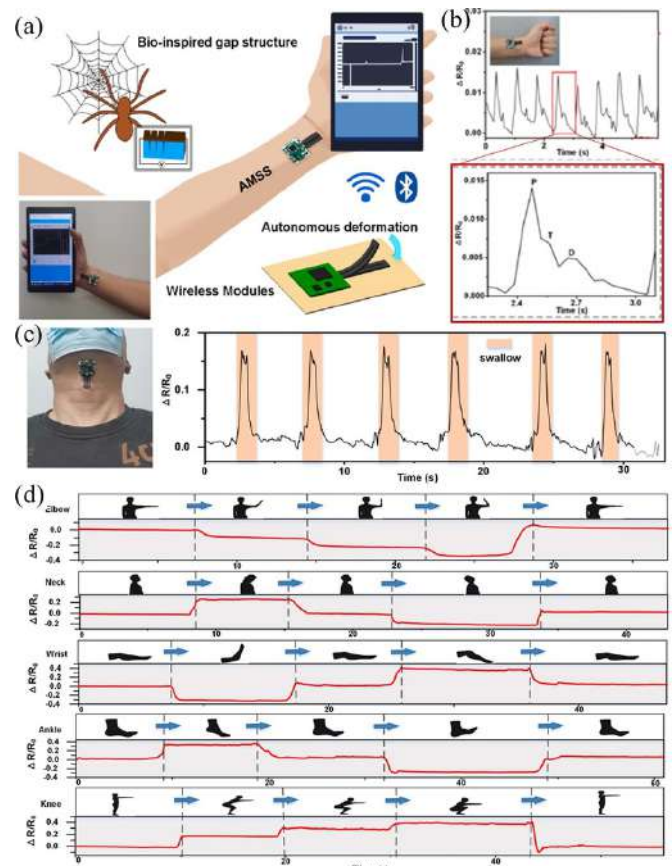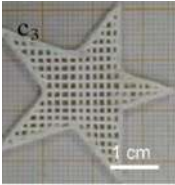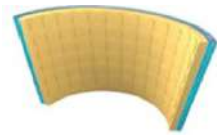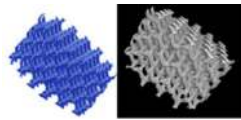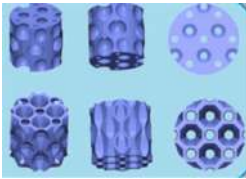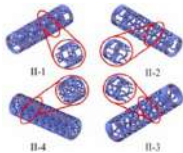

Figure 25. (a) Bionic wearable intelligent electronic device. (b) Pulse monitoring. (c) Swallowing action monitoring. (d) Real-time monitoring of different human movements. Reprinted from [204], © 2024 Elsevier Ltd All rights reserved.
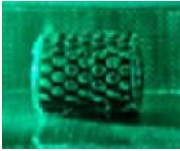
4D printed SMP biomedical devices. Although 4D printing of SMP biomedical devices is still in its infancy, it could become an indispensable method for the rapid manufacturing of dynamically customized biomedical devices and lead to highly meaningful technological updates. In the future, 4D printed SMP intelligent biomedical devices are expected to facilitate major innovations in the fields of tissue engineering scaffolds, living organs, and drug delivery, such as intelligent repair of tissue organs, development of scaffolds that can adapt to physiological growth, real-time accurate disease monitoring and targeted drug delivery to hard-to-reach areas inside the human body.

Table 3. 4D printed SMP biomedical devices.

Biomedical devices	Materials	Stimuli	Printing strategy	Representative device pictures	References
Multiscale porous bioactive bone scaffolds	PLMC-based	Heat	DIW		Reproduced from [193], with permission from Springer Nature.
Multi-responsive membrane for bone healing	PCLDA	Heat	DLP		[66] John Wiley & Sons. © 2021 Wiley-VCH GmbH
Bone scaffolds	PPF	Heat	DLP		Reprinted with permission from [74]. Copyright (2020) American Chemical Society.
Porous bone scaffolds	PLA/Fe$_3$O$_4$	Magnetic field	FDM		Reprinted from [191], © 2020 Elsevier Ltd All rights reserved.
Bionic bone scaffolds	PLA/Fe$_3$O$_4$	Magnetic field	FDM		Reprinted from [104], © 2019 Published by Elsevier Ltd.
Porous bone scaffolds	GO-PBS/PLA	NIR	FDM		Reprinted from [184], © 2021 Elsevier Ltd All rights reserved.
Endoluminal stents	Methacrylated PCL	Heat	SLA		[20] John Wiley & Sons. © 2016 WILEY-VCH Verlag GmbH & Co. KGaA, Weinheim
Bionic tracheal stents	PCL/BPO/Fe$_3$O$_4$	Magnetic field	/		Reprinted from [83], © 2022 Elsevier Ltd All rights reserved.

Table 3. (Continued.)

4D printed remote-controlled tracheal stents	PLA/Fe$_3$O$_4$	Magnetic field	FDM		Reproduced from [196]. CC BY 4.0.
Personalized bioinspired tracheal stents	PLA/Fe$_3$O$_4$	Magnetic field	FDM		Reprinted from [84], © 2019 Elsevier Ltd All rights reserved.
Intraluminal stents	SMPU/AuNPs	Light	DIW		Reprinted with permission from [197]. Copyright (2022) American Chemical Society.
Biodegradable and remotely controllable ASD occlusion devices	PLA/Fe$_3$O$_4$	Magnetic field	FDM		[73] John Wiley & Sons. © 2019 WILEY-VCH Verlag GmbH & Co. KGaA, Weinheim
Bioinspired absorbable LAA occlusion devices	PLA/Fe$_3$O$_4$	Magnetic field	FDM		Reprinted with permission from [190]. Copyright (2021) American Chemical Society.
Cardiac patch for myocardial regeneration	PEGDA/graphene	Light (NIR)	DLP		Reprinted with permission from [81]. Copyright (2021) American Chemical Society.
Negative Poisson's ratio vascular stents	PLA	Heat	FDM		Reproduced from [93], with permission from Springer Nature.
4D active vascular stents	c-PLA/Fe$_3$O$_4$	Magnetic field	DIW		Reprinted with permission from [114]. Copyright (2016) American Chemical Society.

(Continued.)

Table 3. (Continued.)

Biomedical devices	Materials	Stimuli	Printing strategy	Representative device pictures	References
Cell-loaded scaffolds with controlled cell morphology	PVA,PDMS	Heat	FDM, Extrusion, and STL		Reproduced from [80]. CC BY 4.0.
Scaffolds with anisotropic internal morphology	AA-MA/PCL	Water	UV-assisted DIW		Reprinted with permission from [85]. Copyright (2021) American Chemical Society.
Drug-loading deployable biomedical devices	PCL, β-CD, everolimus	Heat	DIW		[2] John Wiley & Sons. © 2022 Wiley-VCH GmbH
Intravesical drug delivery retention device	PVA; PVA/GLY	Water	FDM		Reprinted from [206], © 2019 Elsevier B.V. All rights reserved.
Scaffolds for soft tissue repair	Aliphatic polycarbonate	Heat	DLP		Reproduced from [203]. CC BY 4.0.
3D cell culture tube array	PEGDA-BPA	Heat	PμSL		[72] John Wiley & Sons. © 2020 Wiley-VCH GmbH

Conflict of interest

The authors declare that they have no known competing financial interests or personal relationships that could have appeared to influence the work reported in this paper.

ORCID iD

Yanju Liu ⓘ https://orcid.org/0000-0001-8269-1594

References

[1] Ni C *et al* 2023 Shape memory polymer with programmable recovery onset *Nature* **622** 748–53

[2] He W *et al* 2023 A biocompatible 4D printing shape memory polymer as emerging strategy for fabrication of deployable medical devices *Macromol. Rapid Commun.* **44** 2200553

[3] Wang Y, Zhu M, Hao C, Dai R, Huang M, Liu H, He S and Liu W 2022 Development of semi-crystalline polyurethane with self-healing and body temperature-responsive shape memory properties *Eur. Polym. J.* **167** 111060

[4] Chen C, Hou Z, Chen S, Guo J, Chen Z, Hu J and Yang L 2022 Photothermally responsive smart elastomer composites based on aliphatic polycarbonate backbone for biomedical applications *Composites* B **240** 109985

[5] Pandey H, Mohol S and Kandi R 2022 4D printing of tracheal scaffold using shape-memory polymer composite *Mater. Lett.* **329** 133238

[6] Zhao F, Zheng X, Zhou S, Zhou B, Xue S and Zhang Y 2021 Constitutive model for epoxy shape memory polymer with regulable phase transition temperature *Int. J. Smart Nano Mat.* **12** 72–87

[7] Zare M, Prabhakaran M, Parvin N and Ramakrishna S 2019 Thermally-induced two-way shape memory polymers: mechanisms, structures, and applications *Chem. Eng. J.* **374** 706–20

[8] Ze Q, Kuang X, Wu S, Wong J, Montgomery S, Zhang R, Kovitz J, Yang F, Qi H and Zhao R 2020 Magnetic shape memory polymers with integrated multifunctional shape manipulation *Adv. Mater.* **32** 1906657

[9] Lendlein A and Gould O E C 2019 Reprogrammable recovery and actuation behaviour of shape-memory polymers *Nat. Rev. Mater.* **4** 116–33

[10] Delaey J, Dubruel P and Van Vlierberghe S 2020 Shape-memory polymers for biomedical applications *Adv. Funct. Mater.* **30** 1909047

[11] Zhang W *et al* 2021 Structural multi-colour invisible inks with submicron 4D printing of shape memory polymers *Nat. Commun.* **12** 112

[12] Herath M, Epaarachchi J, Islam M, Fang L and Leng J 2020 Light activated shape memory polymers and composites: a review *Eur. Polym. J.* **136** 109912

[13] Xia Y, He Y, Zhang F, Liu Y and Leng J 2020 A review of shape memory polymers and composites: mechanisms, materials, and applications *Adv. Mater.* **33** 2000713

[14] Xin X, Liu L, Liu Y and Leng J 2019 Mechanical models, structures, and applications of shape-memory polymers and their composites *Acta Mech. Solida Sin.* **32** 535–65

[15] Zhao Q, Li C, Shum H and Du X 2020 Shape-adaptable biodevices for wearable and implantable applications *Lab Chip* **20** 4321–41

[16] Zhao Q, Wang J, Cui H, Chen H, Wang Y and Du X 2018 Programmed shape-morphing scaffolds enabling facile 3D endothelialization *Adv. Funct. Mater.* **28** 1801027

[17] Li Y, Zhang F, Liu Y and Leng J 2020 4D printed shape memory polymers and their structures for biomedical applications *Sci. China Technol. Sci.* **63** 545–60

[18] Lin C, Liu L, Liu Y and Leng J 2020 The compatibility of polylactic acid and polybutylene succinate blends by molecular and mesoscopic dynamics *Int. J. Smart Nano Mater.* **11** 24–37

[19] Senatov F, Niaza K, Zadorozhnyy M, Maksimkin A, Kaloshkin S and Estrin Y 2016 Mechanical properties and shape memory effect of 3D-printed PLA-based porous scaffolds *J. Mech. Behav. Biomed.* **57** 139–48

[20] Zarek M, Mansour N, Shapira S and Cohn D 2017 4D printing of shape memory-based personalized endoluminal medical devices *Macromol. Rapid Commun.* **38** 1600628

[21] Singhal P, Small W, Cosgriff-Hernandez E, Maitland D and Wilson T 2014 Low density biodegradable shape memory polyurethane foams for embolic biomedical applications *Acta Biomater.* **10** 67–76

[22] Lendlein A, Behl M, Hiebl B and Wischke C 2010 Shape-memory polymers as a technology platform for biomedical applications *Expert Rev. Med. Devices* **7** 357–79

[23] Wischke C, Neffe A, Steuer S and Lendlein A 2009 Evaluation of a degradable shape-memory polymer network as matrix for controlled drug release *J. Control. Release* **138** 243–50

[24] Yakacki C and Gall K 2010 Shape-memory polymers for biomedical applications *Shape-Memory Polymers* ed A Lendlein (Springer) pp 147–75

[25] Zhao W, Liu L, Zhang F, Leng J and Liu Y 2019 Shape memory polymers and their composites in biomedical applications *Mater. Sci. Eng.* C **97** 864–83

[26] Xie R, Hu J, Hoffmann O, Zhang Y, Ng F, Qin T and Guo X 2018 Self-fitting shape memory polymer foam inducing bone regeneration: a rabbit femoral defect study *BBA-Gen. Subjects* **1862** 936–45

[27] Stansbury J and Idacavage M 2016 3D printing with polymers: challenges among expanding options and opportunities *Dent. Mater.* **32** 54–64

[28] Kumar R, Kumar M and Chohan J 2021 Material-specific properties and applications of additive manufacturing techniques: a comprehensive review *Bull. Mater. Sci.* **44** 181

[29] Do A, Khorsand B, Geary S and Salem A 2015 3D printing of scaffolds for tissue regeneration applications *Adv. Healthcare Mater.* **4** 1742–62

[30] Zhang C, Li X, Jiang L, Tang D, Xu H, Zhao P, Fu J, Zhou Q and Chen Y 2021 3D printing of functional magnetic materials: from design to applications *Adv. Funct. Mater.* **31** 2102777

[31] Xu W *et al* 2021 3D printing-enabled nanoparticle alignment: a review of mechanisms and applications *Small* **17** 2100817

[32] Kalkal A, Kumar S, Kumar P, Pradhan R, Willander M, Packirisamy G, Kumar S and Malhotra B 2021 Recent advances in 3D printing technologies for wearable (Bio)sensors *Addit. Manuf.* **46** 102088

[33] Zhan Z, Chen L, Duan H, Chen Y, He M and Wang Z 2022 3D printed ultra-fast photothermal responsive shape memory hydrogel for microrobots *Int. J. Extrem. Manuf.* **4** 15302

[34] Song J, Lv B, Chen W, Ding P and He Y 2023 Advances in 3D printing scaffolds for peripheral nerve and spinal cord injury repair *Int. J. Extrem. Manuf.* **5** 32008

[35] Cheng W, Zhang J, Liu J and Yu Z 2020 Granular hydrogels for 3D bioprinting applications *View* **1** 20200060

[36] Liu Z, Zhang M, Bhandari B and Wang Y 2017 3D printing: printing precision and application in food sector *Trends Food Sci. Technol.* **69** 83–94

[37] Browne M, Redondo E and Pumera M 2020 3D printing for electrochemical energy applications *Chem. Rev.* **120** 2783–810

[38] Qin C and Wu C 2022 Inorganic biomaterials-based bioinks for three-dimensional bioprinting of regenerative scaffolds *View* **3** 20210018

[39] Dabbagh S, Sarabi M, Rahbarghazi R, Sokullu E, Yetisen A and Tasoglu S 2021 3D-printed microneedles in biomedical applications *Iscience* **24** 102012

[40] Ambrosi A and Pumera M 2016 3D-printing technologies for electrochemical applications *Chem. Soc. Rev.* **45** 2740–55

[41] Lin C, Huang Z, Wang Q, Wang W, Wang W, Wang Z, Liu L, Liu Y and Leng J 2022 3D printed bioinspired stents with

photothermal effects for malignant colorectal obstruction *Research* **2022** 1–12

[42] Gao Z, Yin J, Liu P, Li Q, Zhang R, Yang H and Zhou H 2023 Simultaneous multi-material embedded printing for 3D heterogeneous structures *Int. J. Extrem. Manuf.* **5** 35001

[43] Vukicevic M, Mosadegh B, Min J and Little S 2017 Cardiac 3D printing and its future directions *JACC Cardiovasc. Imaging* **10** 171–84

[44] Ackland D, Robinson D, Redhead M, Lee P V S, Moskaljuk A and Dimitroulis G 2017 A personalized 3D-printed prosthetic joint replacement for the human temporomandibular joint: from implant design to implantation *J. Mech. Behav. Biomed.* **69** 404–11

[45] Goyanes A, Det-Amornrat U, Wang J, Basit A and Gaisford S 2016 3D scanning and 3D printing as innovative technologies for fabricating personalized topical drug delivery systems *J. Control. Release* **234** 41–48

[46] Jariwala S, Lewis G, Bushman Z, Adair J and Donahue H 2015 3D printing of personalized artificial bone scaffolds *3D Print. Addit. Manuf.* **2** 56–64

[47] Bose S, Vahabzadeh S and Bandyopadhyay A 2013 Bone tissue engineering using 3D printing *Mater. Today* **16** 496–504

[48] Kumar A, Mandal S, Barui S, Vasireddi R, Gbureck U, Gelinsky M and Basu B 2016 Low temperature additive manufacturing of three dimensional scaffolds for bone-tissue engineering applications: processing related challenges and property assessment *Mater. Sci. Eng.* R **103** 1–39

[49] Miao S *et al* 2017 4D printing of polymeric materials for tissue and organ regeneration *Mater. Today* **20** 577–91

[50] Jang J *et al* 2017 3D printed complex tissue construct using stem cell-laden decellularized extracellular matrix bioinks for cardiac repair *Biomaterials* **112** 264–74

[51] Park J, Jang J, Lee J and Cho D 2016 Current advances in three-dimensional tissue/organ printing *Tissue Eng. Regen. Med.* **13** 612–21

[52] Murphy S and Atala A 2014 3D bioprinting of tissues and organs *Nat. Biotechnol.* **32** 773–85

[53] Ryu S *et al* 2015 Nanothin coculture membranes with tunable pore architecture and thermoresponsive functionality for transfer-printable stem cell-derived cardiac sheets *ACS Nano* **9** 10186–202

[54] Tibbits 2013 The emergence of "4D printing" *Ted Conference*

[55] Cui C, An L, Zhang Z, Ji M, Chen K, Yang Y, Su Q, Wang F, Cheng Y and Zhang Y 2022 Reconfigurable 4D printing of reprocessable and mechanically strong polythiourethane covalent adaptable networks *Adv. Funct. Mater.* **32** 2203720

[56] Melocchi A, Uboldi M, Cerea M, Foppoli A, Maroni A, Moutaharrik S, Palugan L, Zema L and Gazzaniga A 2021 Shape memory materials and 4D printing in pharmaceutics *Adv. Drug Deliv. Rev.* **173** 216–37

[57] Alshebly Y, Nafea M, Mohamed Ali M and Almurib H A F 2021 Review on recent advances in 4D printing of shape memory polymers *Eur. Polym. J.* **159** 110708

[58] Andreu A, Su P, Kim J, Cs N, Kim S, Kim I, Lee J, Noh J, Subramanian A and Yoon Y 2021 4D printing materials for vat photopolymerization *Addit. Manuf.* **44** 102024

[59] Ahmed A, Arya S, Gupta V, Furukawa H and Khosla A 2021 4D printing: fundamentals, materials, applications and challenges *Polymer* **228** 123926

[60] Mallakpour S, Tabesh F and Hussain C 2021 3D and 4D printing: from innovation to evolution *Adv. Colloid Interface* **294** 102482

[61] Fu P *et al* 2022 4D printing of polymers: techniques, materials, and prospects *Prog. Polym. Sci.* **126** 101506

[62] Wang Y, Cui H, Esworthy T, Mei D, Wang Y and Zhang L 2022 Emerging 4D printing strategies for next-generation tissue regeneration and medical devices *Adv. Mater.* **34** 2109198

[63] Khorsandi D *et al* 2021 3D and 4D printing in dentistry and maxillofacial surgery: printing techniques, materials, and applications *Acta Biomater.* **122** 26–49

[64] Ryan K, Down M and Banks C 2021 Future of additive manufacturing: overview of 4D and 3D printed smart and advanced materials and their applications *Chem. Eng. J.* **403** 126162

[65] Wang Y, Miao Y, Zhang J, Wu J, Kirk T, Xu J, Ma D and Xue W 2018 Three-dimensional printing of shape memory hydrogels with internal structure for drug delivery *Mater. Sci. Eng.* C **84** 44–51

[66] You D *et al* 2021 4D printing of multi-responsive membrane for accelerated in vivo bone healing via remote regulation of stem cell fate *Adv. Funct. Mater.* **31** 2103920

[67] Zarek M, Layani M, Eliazar S, Mansour N, Cooperstein I, Shukrun E, Szlar A, Cohn D and Magdassi S 2016 4D printing shape memory polymers for dynamic jewellery and fashionwear *Virtual Phys. Prototyp.* **11** 263–70

[68] Zhang Y, Huang L, Song H, Ni C, Wu J, Zhao Q and Xie T 2019 4D printing of a digital shape memory polymer with tunable high performance *ACS Appl. Mater. Interfaces* **11** 32408–13

[69] Choong Y Y C, Maleksaeedi S, Eng H, Wei J and Su P 2017 4D printing of high performance shape memory polymer using stereolithography *Mater. Des.* **126** 219–25

[70] Ge Q, Sakhaei A, Lee H, Dunn C, Fang N and Dunn M 2016 Multimaterial 4D printing with tailorable shape memory polymers *Sci. Rep.* **6** 31110

[71] Bodaghi M, Damanpack A and Liao W 2018 Triple shape memory polymers by 4D printing *Smart Mater. Struct.* **27** 65010

[72] Yang C, Luo J, Polunas M, Bosnjak N, Chueng S-T D, Chadwick M, Sabaawy H, Chester S, Lee K and Lee H 2020 4D-printed transformable tube array for high-throughput 3D cell culture and histology *Adv. Mater.* **32** 2004285

[73] Lin C, Lv J, Li Y, Zhang F, Li J, Liu Y, Liu L and Leng J 2019 4D-printed biodegradable and remotely controllable shape memory occlusion devices *Adv. Funct. Mater.* **29** 1906569

[74] Le Fer G and Becker M 2020 4D printing of resorbable complex shape-memory poly(propylene fumarate) star scaffolds *ACS Appl. Mater. Interfaces* **12** 22444–52

[75] Abdullah T and Okay O 2023 4D printing of body temperature-responsive hydrogels based on poly(acrylic acid) with shape-memory and self-healing abilities *ACS Appl. Bio Mater.* **6** 703–11

[76] Lyu Z, Wang J and Chen Y 2023 4D printing: interdisciplinary integration of smart materials, structural design, and new functionality *Int. J. Extrem. Manuf.* **5** 32011

[77] Chen A, Su J, Li Y, Zhang H, Shi Y, Yan C and Lu J 2023 3D/4D printed bio-piezoelectric smart scaffolds for next-generation bone tissue engineering *Int. J. Extrem. Manuf.* **5** 032007

[78] Deng Y, Yang B, Zhang F, Liu Y, Sun J, Zhang S, Zhao Y, Yuan H and Leng J 2022 4D printed orbital stent for the treatment of enophthalmic invagination *Biomaterials* **291** 121886

[79] Zhang C, Cai D, Liao P, Su J, Deng H, Vardhanabhuti B, Ulery B, Chen S and Lin J 2021 4D printing of shape-memory polymeric scaffolds for adaptive biomedical implantation *Acta Biomater.* **122** 101–10

[80] Miao S, Cui H, Esworthy T, Mahadik B, Lee S, Zhou X, Hann S Y, Fisher J P and Zhang L G 2020 4D

self-morphing culture substrate for modulating cell differentiation *Adv. Sci.* **7** 1902403

[81] Wang Y, Cui H, Wang Y, Xu C, Esworthy T, Hann S, Boehm M, Shen Y, Mei D and Zhang L 2021 4D printed cardiac construct with aligned myofibers and adjustable curvature for myocardial regeneration *ACS Appl. Mater. Interfaces* **13** 12746–58

[82] Hendrikson W, Rouwkema J, Clementi F, Van Blitterswijk C, Farè S and Moroni L 2017 Towards 4D printed scaffolds for tissue engineering: exploiting 3D shape memory polymers to deliver time-controlled stimulus on cultured cells *Biofabrication* **9** 31001

[83] Zhao W, Huang Z, Liu L, Wang W, Leng J and Liu Y 2022 Bionic design and performance research of tracheal stent based on shape memory polycaprolactone *Compos. Sci. Technol.* **229** 109671

[84] Zhao W, Zhang F, Leng J and Liu Y 2019 Personalized 4D printing of bioinspired tracheal scaffold concept based on magnetic stimulated shape memory composites *Compos. Sci. Technol.* **184** 107866

[85] Constante G, Apsite I, Alkhamis H, Dulle M, Schwarzer M, Caspari A, Synytska A, Salehi S and Ionov L 2021 4D biofabrication using a combination of 3D printing and melt-electrowriting of shape-morphing polymers *ACS Appl. Mater. Interfaces* **13** 12767–76

[86] Li Y, You J, Lv H, Wang C, Zhai S, Ren S, Liu X, Zhang Y and Zhou Y 2024 4D-printed dual-responsive bioscaffolds for treating critical-sized irregular bone defects *Chem. Eng J.* **489** 151205

[87] Cheng C-Y, Xie H, Xu Z, Li L, Jiang M-N, Tang L, Yang K-K and Wang Y-Z 2020 4D printing of shape memory aliphatic copolyester via UV-assisted FDM strategy for medical protective devices *Chem. Eng J.* **396** 125242

[88] Wang W, Liu Y and Leng J 2016 Recent developments in shape memory polymer nanocomposites: actuation methods and mechanisms *Coord. Chem. Rev.* **320-321** 38–52

[89] Bai Y, Liu J, Ju J and Chen X 2021 Novel near-infrared light-induced triple-shape memory composite based on poly(ethylene-co-vinyl alcohol) and iron tannate *ACS Appl. Mater. Interfaces* **13** 23011–9

[90] Shi S, Cui M, Sun F, Zhu K, Iqbal M I, Chen X, Fei B, Li R K Y, Xia Q and Hu J 2021 An Innovative solvent-responsive coiling–expanding stent *Adv. Mater.* **33** 2101005

[91] Xiang T, Wang J, Jia L, Wang P and Zhou S 2022 Semicrystalline polymer networks with a swelling-enhanced water-triggered two-way shape-memory effect for programmable deformation and smart actuation *Polym. Chem.* **13** 6614–24

[92] Chi D, Gu H, Wang J, Wu C, Wang R, Cheng Z, Zhang D, Xie Z and Liu Y 2023 Narrow response temperature range with excellent reversible shape memory effect for semi-crystalline networks as soft actuators *Mater. Horiz.* **10** 2464–75

[93] Lin C, Zhang L, Liu Y, Liu L and Leng J 2020 4D printing of personalized shape memory polymer vascular stents with negative poisson's ratio structure: a preliminary study *Sci. China Technol. Sci.* **63** 578–88

[94] Khalid M, Arif Z, Noroozi R, Zolfagharian A and Bodaghi M 2022 4D printing of shape memory polymer composites: a review on fabrication techniques, applications, and future perspectives *J. Manuf. Process.* **81** 759–97

[95] Xie Y, Lei D, Wang S, Liu Z, Sun L, Zhang J, Qing F, He C and You Z 2019 A biocompatible, biodegradable, and functionalizable copolyester and its application in water-responsive shape memory scaffold *ACS Biomater. Sci. Eng.* **5** 1668–76

[96] Rose A, Zhu Z, Madigan C, Swager T and Bulović V 2005 Sensitivity gains in chemosensing by lasing action in organic polymers *Nature* **434** 876–9

[97] Salvekar A, Huang W, Xiao R, Wong Y, Venkatraman S, Tay K and Shen Z 2017 Water-responsive shape recovery induced buckling in biodegradable photo-cross-linked poly(ethylene glycol) (PEG) hydrogel *Acc. Chem. Res.* **50** 141–50

[98] Xie H *et al* 2018 Biodegradable near-infrared-photoresponsive shape memory implants based on black phosphorus nanofillers *Biomaterials* **164** 11–21

[99] Fang L, Fang T, Liu X, Ni Y, Lu C and Xu Z 2017 Precise stimulation of near-infrared light responsive shape-memory polymer composites using upconversion particles with photothermal capability *Compos. Sci. Technol.* **152** 190–7

[100] Schmidt A 2006 Electromagnetic activation of shape memory polymer networks containing magnetic nanoparticles *Macromol. Rapid Commun.* **27** 1168–72

[101] Li S, Jin X, Shao Y, Qi X, Yang J and Wang Y 2019 Gold nanoparticle/reduced graphene oxide hybrids for fast light-actuated shape memory polymers with enhanced photothermal conversion and mechanical stiffness *Eur. Polym. J.* **116** 302–10

[102] Lu H, Min Huang W, Fu Y Q and Leng J 2014 Quantitative separation of the influence of hydrogen bonding of ethanol water mixture on the shape recovery behavior of polyurethane shape memory polymer *Smart Mater. Struct.* **23** 125041

[103] Fang C, Kievit F, Veiseh O, Stephen Z, Wang T, Lee D, Ellenbogen R and Zhang M 2012 Fabrication of magnetic nanoparticles with controllable drug loading and release through a simple assembly approach *J. Control. Release* **162** 233–41

[104] Zhang F, Wang L, Zheng Z, Liu Y and Leng J 2019 Magnetic programming of 4D printed shape memory composite structures *Composites* A **125** 105571

[105] Li Y, Huang G, Zhang X, Li B, Chen Y, Lu T, Lu T J and Xu F 2013 Magnetic hydrogels and their potential biomedical applications *Adv. Funct. Mater.* **23** 660–72

[106] Apaj Q, Connolly J, Jones S K and Dobson J 2003 Applications of magnetic nanoparticles in biomedicine *J. Phys. D: Appl. Phys.* **36** R167

[107] Yu S, Li G, Liu R, Ma D and Xue W 2018 Dendritic Fe_3O_4@Poly(dopamine)@PAMAM nanocomposite as controllable NO-releasing material: a synergistic photothermal and NO antibacterial study *Adv. Funct. Mater.* **28** 1707440

[108] Cezar C, Kennedy S, Mehta M, Weaver J, Gu L, Vandenburgh H and Mooney D 2014 Biphasic ferrogels for triggered drug and cell delivery *Adv. Healthcare Mater.* **3** 1869–76

[109] Wang Y, Ye J and Tian W 2016 Shape memory polymer composites of Poly(styrene-b-butadiene-b-styrene) copolymer/liner low density polyethylene/Fe_3O_4 nanoparticles for remote activation *Appl. Sci.* **6** 333

[110] Guo Q, Bishop C, Meyer R, Wilson D, Olasov L, Schlesinger D, Mather P, Spicer J, Elisseeff J and Green J 2018 Entanglement-based thermoplastic shape memory polymeric particles with photothermal actuation for biomedical applications *ACS Appl. Mater. Interfaces* **10** 13333–41

[111] Lahikainen M, Zeng H and Priimagi A 2018 Reconfigurable photoactuator through synergistic use of photochemical and photothermal effects *Nat. Commun.* **9** 4148

[112] Li S, Tu Y, Bai H, Hibi Y, Wiesner L, Pan W, Wang K, Giannelis E and Shepherd R 2019 Simple synthesis of

elastomeric photomechanical switches that self-heal *Macromol. Rapid Commun.* **40** 1970009

[113] Wie J, Shankar M and White T 2016 Photomotility of polymers *Nat. Commun.* **7** 13260

[114] Wei H, Zhang Q, Yao Y, Liu L, Liu Y and Leng J 2016 Direct-write fabrication of 4D active shape-changing structures based on a shape memory polymer and its nanocomposite *ACS Appl. Mater. Interfaces* **9** 876–83

[115] Tao W *et al* 2017 Black phosphorus nanosheets as a robust delivery platform for cancer theranostics *Adv. Mater.* **29** 1603276

[116] Chen W *et al* 2017 Black phosphorus nanosheet-based drug delivery system for synergistic photodynamic/photothermal/chemotherapy of cancer *Adv. Mater.* **29** 1603864

[117] Shi X, Gong H, Li Y, Wang C, Cheng L and Liu Z 2013 Graphene-based magnetic plasmonic nanocomposite for dual bioimaging and photothermal therapy *Biomaterials* **34** 4786–93

[118] Ma H *et al* 2016 A bifunctional biomaterial with photothermal effect for tumor therapy and bone regeneration *Adv. Funct. Mater.* **26** 1197–208

[119] Liu W *et al* 2022 Water-triggered stiffening of shape-memory polyurethanes composed of hard backbone dangling PEG soft segments *Adv. Mater.* **34** 2201914

[120] Liu Y, Li Y, Chen H, Yang G, Zheng X and Zhou S 2014 Water-induced shape-memory Poly(d,l-lactide)/microcrystalline cellulose composites *Carbohyd. Polym.* **104** 101–8

[121] Zhang F, Xia Y, Wang L, Liu L, Liu Y and Leng J 2018 Conductive shape memory microfiber membranes with core–shell structures and electroactive performance *ACS Appl. Mater. Interfaces* **10** 35526–32

[122] Wang L, Gramlich W and Gardner D 2017 Improving the impact strength of Poly(lactic acid) (PLA) in fused layer modeling (FLM) *Polymer* **114** 242–8

[123] Boparai K, Singh R and Singh H 2016 Development of rapid tooling using fused deposition modeling: a review *Rapid Prototyp. J.* **22** 281–99

[124] Wang J, Xie H, Weng Z, Senthil T and Wu L 2016 A novel approach to improve mechanical properties of parts fabricated by fused deposition modeling *Mater. Des.* **105** 152–9

[125] Penumakala P, Santo J and Thomas A 2020 A critical review on the fused deposition modeling of thermoplastic polymer composites *Composites* B **201** 108336

[126] Smith W and Dean R W 2013 Structural characteristics of fused deposition modeling polycarbonate material *Polym. Test* **32** 1306–12

[127] Liang K, Carmone S, Brambilla D and Leroux J-C 2018 3D printing of a wearable personalized oral delivery device: a first-in-human study *Sci. Adv.* **4** t2544

[128] Wu H, Wang O, Tian Y, Wang M, Su B, Yan C, Zhou K and Shi Y 2021 Selective laser sintering-based 4D printing of magnetism-responsive grippers *ACS Appl. Mater. Interfaces* **13** 12679–88

[129] Arif Z, Khalid M, Ur Rehman E, Ullah S, Atif M and Tariq A 2021 A review on laser cladding of high-entropy alloys, their recent trends and potential applications *J. Manuf. Process.* **68** 225–73

[130] Feng P, Zhao R, Yang F, Peng S, Pan H and Shuai C 2024 Co-continuous structure enhanced magnetic responsive shape memory PLLA/TPU blend fabricated by 4D printing *Virtual Phys. Prototyp.* **19** e2290186

[131] Alsharif A, Aviles J, Zechel F, Alsharif N and El-Atab N 2024 Multi-material direct-ink-writing of silver-based flexible and highly deformable dry electrocardiogram biopatches *View* **5** 20240008

[132] Smith P, Basu A, Saha A and Nelson A 2018 Chemical modification and printability of shear-thinning hydrogel inks for direct-write 3D printing *Polymer* **152** 42–50

[133] Neumann T and Dickey M 2020 Liquid metal direct write and 3D printing: a review *Adv. Mater. Technol.* **5** 2000070

[134] Adib A, Sheikhi A, Shahhosseini M, Simeunović A, Wu S, Castro C, Zhao R, Khademhosseini A and Hoelzle D 2020 Direct-write 3D printing and characterization of a GelMA-based biomaterial for intracorporeal tissue engineering *Biofabrication* **12** 45006

[135] Patel B, Walsh D, Kim D, Kwok J, Lee B, Guironnet D and Diao Y 2020 Tunable structural color of bottlebrush block copolymers through direct-write 3D printing from solution *Sci. Adv.* **6** z7202

[136] Qian F *et al* 2019 Direct writing of tunable living inks for bioprocess intensification *Nano Lett.* **19** 5829–35

[137] Gu Y, Park D, Bowen D, Das S and Hines D 2019 Direct-write printed, solid-core solenoid inductors with commercially relevant inductances *Adv. Mater. Technol.* **4** 1800312

[138] Solís Pinargote N, Smirnov A, Peretyagin N, Seleznev A and Peretyagin P 2020 Direct ink writing technology (3D printing) of graphene-based ceramic nanocomposites: a review *Nanomaterials* **10** 1300

[139] Cheng Y, Chan K, Wang X, Ding T, Li T, Lu X and Ho G 2019 Direct-ink-write 3D printing of hydrogels into biomimetic soft robots *ACS Nano* **13** 13176–84

[140] Hmeidat N, Kemp J and Compton B 2018 High-strength epoxy nanocomposites for 3D printing *Compos. Sci. Technol.* **160** 9–20

[141] Gao Y, Li Q, Wu R, Sha J, Lu Y and Xuan F 2019 Laser direct writing of ultrahigh sensitive sic-based strain sensor arrays on elastomer toward electronic skins *Adv. Funct. Mater.* **29** 1806786

[142] Sanders P, Young A, Qin Y, Fancey K, Reithofer M, Guillet-Nicolas R, Kleitz F, Pamme N and Chin J 2019 Stereolithographic 3D printing of extrinsically self-healing composites *Sci. Rep.* **9** 388

[143] Wadsworth P, Nelson I, Porter D, Raeymaekers B and Naleway S 2020 Manufacturing bioinspired flexible materials using ultrasound directed self-assembly and 3D printing *Mater. Des.* **185** 108243

[144] Peng X, Kuang X, Roach D, Wang Y, Hamel C, Lu C and Qi H 2021 Integrating digital light processing with direct ink writing for hybrid 3D printing of functional structures and devices *Addit. Manuf.* **40** 101911

[145] Wei T, Ahn B, Grotto J and Lewis J 2018 3D printing of customized Li-ion batteries with thick electrodes *Adv. Mater.* **30** 1703027

[146] Patel D, Cohen B, Etgar L and Magdassi S 2018 Fully 2D and 3D printed anisotropic mechanoluminescent objects and their application for energy harvesting in the dark *Mater. Horiz.* **5** 708–14

[147] Neumann T, Facchine E, Leonardo B, Khan S and Dickey M 2020 Direct write printing of a self-encapsulating liquid metal–silicone composite *Soft Matter* **16** 6608–18

[148] Yoon Y, Kim S, Kim D, Kauh S and Lee J 2019 Four degrees-of-freedom direct writing of liquid metal patterns on uneven surfaces *Adv. Mater. Technol.* **4** 1800379

[149] Nan B, Galindo-Rosales F and Ferreira J M F 2020 3D printing vertically: direct ink writing free-standing pillar arrays *Mater. Today* **35** 16–24

[150] Wan X, He Y, Liu Y and Leng J 2022 4D printing of multiple shape memory polymer and nanocomposites with biocompatible, programmable and selectively actuated properties *Addit. Manuf.* **53** 102689

[151] Geraili A, Xing M and Mequanint K 2021 Design and fabrication of drug-delivery systems toward adjustable

release profiles for personalized treatment *View* **2** 20200126

[152] Cui H *et al* 2020 4D physiologically adaptable cardiac patch: a 4-month *in vivo* study for the treatment of myocardial infarction *Sci. Adv.* **6** b5067

[153] Ronca A, Ambrosio L and Grijpma D 2013 Preparation of designed Poly(d,l-lactide)/nanosized hydroxyapatite composite structures by stereolithography *Acta Biomater.* **9** 5989–96

[154] Melchels F P W, Feijen J and Grijpma D 2010 A review on stereolithography and its applications in biomedical engineering *Biomaterials* **31** 6121–30

[155] Bozkurt Y and Karayel E 2021 3D printing technology; methods, biomedical applications, future opportunities and trends *J. Mater. Res. Technol.* **14** 1430–50

[156] Xu X, Goyanes A, Trenfield S, Diaz-Gomez L, Alvarez-Lorenzo C, Gaisford S and Basit A 2021 Stereolithography (SLA) 3D printing of a bladder device for intravesical drug delivery *Mater. Sci. Eng.* C **120** 111773

[157] Zhang J, Hu Q, Wang S, Tao J and Gou M 2020 Digital light processing based three-dimensional printing for medical applications *Int. J. Bioprinting* **6** 242

[158] Bao Y, Paunović N, Franzen D, Studart A and Leroux J 2021 Digital light 3D printing of biodegradable elastomers for personalized devices *CHIMIA Int. J. Chem.* **75** 438

[159] Kim S *et al* 2018 Precisely printable and biocompatible silk fibroin bioink for digital light processing 3D printing *Nat. Commun.* **9** 1620

[160] Traugutt N, Mistry D, Luo C, Yu K, Ge Q and Yakacki C 2020 Liquid-crystal-elastomer-based dissipative structures by digital light processing 3D printing *Adv. Mater.* **32** 2000797

[161] Mao Q, Wang Y, Li Y, Juengpanich S, Li W, Chen M, Yin J, Fu J and Cai X 2020 Fabrication of liver microtissue with liver decellularized extracellular matrix (DECM) bioink by digital light processing (DLP) bioprinting *Mater. Sci. Eng.* C **109** 110625

[162] Lantean S, Barrera G, Pirri C, Tiberto P, Sangermano M, Roppolo I and Rizza G 2019 3D printing of magnetoresponsive polymeric materials with tunable mechanical and magnetic properties by digital light processing *Adv. Mater. Technol.* **4** 1900505

[163] Hong H *et al* 2020 Digital light processing 3D printed silk fibroin hydrogel for cartilage tissue engineering *Biomaterials* **232** 119679

[164] Dean D, Wallace J, Siblani A, Wang M, Kim K, Mikos A and Fisher J 2012 Continuous digital light processing (CDLP): highly accurate additive manufacturing of tissue engineered bone scaffolds *Virtual Phys. Prototyp.* **7** 13–24

[165] Ge Q, Li Z, Wang Z, Kowsari K, Zhang W, He X, Zhou J and Fang N 2020 Projection micro stereolithography based 3D printing and its applications *Int. J. Extrem. Manuf.* **2** 22004

[166] Behroodi E, Latifi H, Bagheri Z, Ermis E, Roshani S and Salehi Moghaddam M 2020 A combined 3D printing/CNC micro-milling method to fabricate a large-scale microfluidic device with the small size 3D architectures: an application for tumor spheroid production *Sci. Rep.* **10** 22171

[167] Han D, Lu Z, Chester S and Lee H 2018 Micro 3D printing of a temperature-responsive hydrogel using projection micro-stereolithography *Sci. Rep.* **8** 1963

[168] Grigoryan B *et al* 2019 Multivascular networks and functional intravascular topologies within biocompatible hydrogels *Science* **364** 458–64

[169] Dominguez-Robles J *et al* 2022 TPU-based antiplatelet cardiovascular prostheses prepared using fused deposition modelling *Mater. Des.* **220** 110837

[170] Vidakis N, Petousis M, Michailidis N, David C, Mountakis N, Papadakis V, Sfakiotakis E, Sagris D, Spiridaki M and Argyros A 2023 Optimized PCL/CNF bio-nanocomposites for medical bio-plotted applications: rheological, structural, and thermomechanical aspects *Bioprinting* **36** e311

[171] Lin C, Huang Z, Wang Q, Zou Z, Wang W, Liu L, Liu Y and Leng J 2023 Mass-producible near-body temperature-triggered 4D printed shape memory biocomposites and their application in biomimetic intestinal stents *Composites* B **256** 110623

[172] Lin C, Huang Z, Wang Q, Zou Z, Wang W, Liu L, Liu Y and Leng J 2023 4D printing of overall radiopaque customized bionic occlusion devices *Adv. Healthcare Mater.* **12** 2201999

[173] Li Y, Chen L, Stehle Y, Lin M, Wang C, Zhang R, Huang M, Li Y and Zou Q 2024 Extrusion-based 3D-printed "rolled-up" composite scaffolds with hierarchical pore structure for bone growth and repair *J. Mater. Sci. Technol.* **171** 222–34

[174] Tay R, Song Y, Yao D and Gao W 2023 Direct-ink-writing 3D-printed bioelectronics *Mater. Today* **71** 135–51

[175] Triacca A, Pitzanti G, Mathew E, Conti B, Dorati R and Lamprou D 2022 Stereolithography 3D printed implants: a preliminary investigation as potential local drug delivery systems to the ear *Int. J. Pharm.* **616** 121529

[176] Field J, Haycock J, Boissonade F and Claeyssens F 2021 A tuneable, photocurable, poly(caprolactone)-based resin for tissue engineering—synthesis, characterisation and use in stereolithography *Molecules* **26** 1199

[177] Sakunphokesup K, Aumnate C and Potiyaraj P 2022 Bio-based resin/cellulose composites for UV-assisted 3D printed orthopedic casts *J. Phys.: Conf. Ser.* **2175** 12007

[178] Song P *et al* 2022 DLP fabricating of precision GelMA/HAP porous composite scaffold for bone tissue engineering application *Composites* B **244** 110163

[179] Gong J *et al* 2022 Digital light processing (DLP) in tissue engineering: from promise to reality, and perspectives *Biomed. Mater.* **17** 62004

[180] Bagheri Saed A, Behravesh A, Hasannia S, Alavinasab Ardebili S, Akhoundi B and Pourghayoumi M 2020 Functionalized poly l-lactic acid synthesis and optimization of process parameters for 3D printing of porous scaffolds via digital light processing (DLP) method *J. Manuf. Process.* **56** 550–61

[181] Dubbin K *et al* 2021 Projection microstereolithographic microbial bioprinting for engineered biofilms *Nano Lett.* **21** 1352–9

[182] Wang Y, Li X, Fan S, Feng X, Cao K, Ge Q, Gao L and Lu Y 2021 Three-dimensional stretchable microelectronics by projection microstereolithography (P*µ*SL) *ACS Appl. Mater. Interfaces* **13** 8901–8

[183] Zhang W, Ye H, Feng X, Zhou W, Cao K, Li M, Fan S and Lu Y 2022 Tailoring mechanical properties of P*µ*SL 3D-printed structures via size effect *Int. J. Extrem. Manuf.* **4** 45201

[184] Lin C, Liu L, Liu Y and Leng J 2022 4D printing of shape memory polybutylene succinate/polylactic acid (PBS/PLA) and its potential applications *Compos. Struct.* **279** 114729

[185] Xin X, Liu L, Liu Y and Leng J 2020 4D printing auxetic metamaterials with tunable, programmable, and reconfigurable mechanical properties *Adv. Funct. Mater.* **30** 2004226

[186] Xin X, Wang Z, Zeng C, Lin C, Liu L, Liu Y and Leng J 2024 4D printing bio-inspired chiral metamaterials for flexible sensors *Composites* B **286** 111761

[187] Liu B *et al* 2024 4D printed hydrogel scaffold with swelling-stiffening properties and programmable

deformation for minimally invasive implantation *Nat. Commun.* **15** 1587

[188] Li N, Liu L, Liu Y and Leng J 2024 Metamaterial-based electronic skin with conformality and multisensory integration *Adv. Funct. Mater.* 2406789

[189] Ren L, Wang Z, Ren L, Han Z, Zhou X, Song Z and Liu Q 2023 4D printing of shape-adaptive tactile sensor with tunable sensing characteristics *Composites* B **265** 110959

[190] Lin C, Liu L, Liu Y and Leng J 2021 4D printing of bioinspired absorbable left atrial appendage occluders: a proof-of-concept study *ACS Appl. Mater. Interfaces* **13** 12668–78

[191] Zhao W, Huang Z, Liu L, Wang W, Leng J and Liu Y 2020 Porous bone tissue scaffold concept based on shape memory PLA/Fe$_3$O$_4$ *Compos. Sci. Technol.* **203** 108563

[192] Chen X, Han S, Wu W, Wu Z, Yuan Y, Wu J and Liu C 2022 Harnessing 4D printing bioscaffolds for advanced orthopedics *Small* **18** 2106824

[193] Wang J, Gao H, Hu Y, Zhang N, Zhou W, Wang C, Binks B and Yang Z 2021 3D printing of pickering emulsion inks to construct poly(D,L-lactide-co-trimethylene carbonate)-based porous bioactive scaffolds with shape memory effect *J. Mater. Sci.* **56** 731–45

[194] Wang C *et al* 2020 Advanced reconfigurable scaffolds fabricated by 4D printing for treating critical-size bone defects of irregular shapes *Biofabrication* **12** 45025

[195] Guo W, Zhou B, Zou Y and Lu X 2024 4D printed poly(l-lactide)/(FeCl$_3$–TA/MgO) composite scaffolds with near-infrared light-induced shape-memory effect and antibacterial properties *Adv. Eng. Mater.* **26** 2301381

[196] Zhang F, Wen N, Wang L, Bai Y and Leng J 2021 Design of 4D printed shape-changing tracheal stent and remote controlling actuation *Int. J. Smart Nano Mater.* **12** 375–89

[197] Deng Y, Zhang F, Jiang M, Liu Y, Yuan H and Leng J 2022 Programmable 4D printing of photoactive shape memory composite structures *ACS Appl. Mater. Interfaces* **14** 42568–77

[198] Shao Z *et al* 2021 Recent progress in biomaterials for heart valve replacement: structure, function, and biomimetic design *View* **2** 20200142

[199] Miao S *et al* 2018 Photolithographic-stereolithographic-tandem fabrication of 4D smart scaffolds for improved stem cell cardiomyogenic differentiation *Biofabrication* **10** 35007

[200] Ma S, Jiang Z, Wang M, Zhang L, Liang Y, Zhang Z, Ren L and Ren L 2021 4D printing of PLA/PCL shape memory composites with controllable sequential deformation *Bio-Des. Manuf.* **4** 867–78

[201] Vakil A, Ramezani M and Monroe M B B 2022 Magnetically actuated shape memory polymers for on-demand drug delivery *Materials* **15** 7279

[202] Zhang F, Zhao T, Ruiz-Molina D, Liu Y, Roscini C, Leng J and Smoukov S K 2020 Shape memory polyurethane microcapsules with active deformation *ACS Appl. Mater. Interfaces* **47059** 47064

[203] Weems A, Arno M, Yu W, Huckstepp R T R and Dove A 2021 4D polycarbonates via stereolithography as scaffolds for soft tissue repair *Nat. Commun.* **12** 3771

[204] Zhang J, Yang X, Li W, Liu H, Yin Z, Chen Y and Zhou X 2024 4D printed multifunctional wearable strain sensors with programmable sensing characteristics *Composites* B **275** 111346

[205] Li N, Zhao W, Li F, Liu L, Liu Y and Leng J 2023 A 4D-printed programmable soft network with fractal design and adjustable hydrophobic performance *Matter* **6** 940–62

[206] Melocchi A, Inverardi N, Uboldi M, Baldi F, Maroni A, Pandini S, Briatico-Vangosa F, Zema L and Gazzaniga A 2019 Retentive device for intravesical drug delivery based on water-induced shape memory response of poly(Vinyl alcohol): design concept and 4D printing feasibility *Int. J. Pharm.* **559** 299–311